NPS 69-85-007PR

NAVAL POSTGRADUATE SCHOOL

Monterey, California

GEOMETRICALLY NONLINEAR ANALYSIS OF SHELL STRUCTURES USING FLAT DKT SHELL ELEMENTS

by

Jean-Louis Batoz and Gilles Cantin

November 1985

Progress Report for period
Oct 1984 - Sep 85

Approved for public release; distribution unlimited.

Prepared for:
David W. Taylor Naval Ship
Research and Development Center
Bethesda, MD 20084

NAVAL POSTGRADUATE SCHOOL
Monterey, California

RADM R. H. Shumaker
Superintendent

D. A. Schrady
Provost

The work reported herein was supported by the David W. Taylor Naval Ship Research and Development Center through work request N00167-85-WR5-0372.

 This report was prepared by:

REPORT DOCUMENTATION PAGE

READ INSTRUCTIONS BEFORE COMPLETING FORM

1. REPORT NUMBER: NPS 69-85-007PR	2. GOVT ACCESSION NO.
3. RECIPIENT'S CATALOG NUMBER	
4. TITLE (and Subtitle): GEOMETRICALLY NONLINEAR ANALYSIS OF SHELL STRUCTURES USING FLAT DKT SHELL ELEMENTS	5. TYPE OF REPORT & PERIOD COVERED: Progress Report 01 Oct 84 - 30 Sep 85
	6. PERFORMING ORG. REPORT NUMBER
7. AUTHOR(s): Jean-Louis Batoz and Gilles Cantin	8. CONTRACT OR GRANT NUMBER(s): N00167-85-WR5-0372
9. PERFORMING ORGANIZATION NAME AND ADDRESS: Naval Postgraduate School, Monterey, CA 93943-5100	10. PROGRAM ELEMENT, PROJECT, TASK AREA & WORK UNIT NUMBERS
11. CONTROLLING OFFICE NAME AND ADDRESS: David W. Taylor Naval Ship Research and Development Center, Bethesda, MD 20084	12. REPORT DATE: 22 November 1985
	13. NUMBER OF PAGES: 64
14. MONITORING AGENCY NAME & ADDRESS(if different from Controlling Office)	15. SECURITY CLASS. (of this report): Unclassified
	15a. DECLASSIFICATION/DOWNGRADING SCHEDULE

16. DISTRIBUTION STATEMENT (of this Report)

Approved for public release; distribution unlimited.

17. DISTRIBUTION STATEMENT (of the abstract entered in Block 20, if different from Report)

18. SUPPLEMENTARY NOTES

19. KEY WORDS (Continue on reverse side if necessary and identify by block number)

Finite elements; numerical analysis; shell structures; nonlinear algorithms

20. ABSTRACT (Continue on reverse side if necessary and identify by block number)

This report describes nonlinear analysis of arbitrary thin shell structures subjected to static loads. The nonlinear analysis includes pre and post-buckling behavior for any degree of non-linearity due to large displacements and large rotations but small strains. The formulation includes some recent developments of plate and shell theories, automatic solution strategies for the nonlinear equations; all adapted for implementation in mini and micro-computers with virtual memory.

GEOMETRICALLY NONLINEAR ANALYSIS OF SHELL STRUCTURES USING FLAT DKT SHELL ELEMENTS

1. INTRODUCTION

Pressure vessels and naval structures are obtained by specific assemblage of plate and shell panels. The knowledge of the behavior of these structural components is essential if optimum design and integrity of the overall structure for a given set of parameters are sought. [1], [2]

This report deals with the nonlinear analysis of arbitrary thin shell structures subjected to static loads. The nonlinear analysis includes pre and post-buckling behavior for any degree of nonlinearity due to large displacements and large rotations, but small strains.

Despite the important research and development efforts made since the beginning of the finite element method era, the analysis of shell structures is still an open active research subject. The following questions are still actively investigated:

- how to approximate the real three dimensional problem?
- what type of finite element discretization is most appropriate?
- how to solve accurately and efficiently the nonlinear equations in various situations of pre and post-buckling?
- how practical and general is the computer code that aimed to solve the problem and what are its computer resource needs?

The object of our report is to present a formulation which includes some recent developments on nonlinear continuum mechanics, plate and shell finite elements, automatic solution and strategies for nonlinear equations and to present the possibilities of a computer code that is adapted for mini and micro-computers to solve moderately small size shell problems.

The nonlinear formulations considered are a Total and an Updated Lagrangian formulations [3], [4], [5] combined with flat simple triangular elements having only 3 nodes and the 6 engineering degrees of freedom at the nodes. The shell finite element is obtained from the superposition of the CST and the DKT plate bending element known to be very efficient, reliable and effective for all thin plate bending analysis. [6], [7], [8], [9], [10], [11]. The nonlinear equations are solved using various methods and strategies based on the full or modified Newton-Raphson method to deal with the automatic determination of the pre and post-buckling load displacement curves. Three basic strategies are considered: the load incrementation, the displacement control method [12], [13], and the arc-length control method [14], [15], [16], [17], [18]. The FORTRAN 77 routines dealing with the shell element and the nonlinear solution procedures are compatible with the documented computer code MEF presented in detail in [19]. The numerical examples presented in this report have been obtained using a VAX 11/750, a VAX 11/780 and an APOLLO/DN300.

The Lagrangian Formulations (TLF and ULF) considered in this report are discussed in chapter 1. The DKT18 triangular shell element is described in chapter 2. The solution strategy to deal with the automatic determination of the load deflection curves is presented in chapter 3. The numerical results are discussed in chapter 4. They deal with nonlinear behavior, buckling, post-buckling and large rotations of elastic shells subjected to one variable load parameter.

2. THE LAGRANGIAN FORMULATIONS FOR NONLINEAR SHELL ANALYSIS

2.1 Different configurations of a shell in space.

We consider a shell structure with a fixed orthogonal coordinate system XYZ (Fig. 1):

- ${}^{0}\Gamma$ refers to the undeformed (initial) configuration
- ${}^{1}\Gamma$ refers to a deformed (intermediate) configuration in equilibrium under a given set of loads ${}^{1}\vec{f}$
- Γ refers to a deformed (final) configuration in equilibrium under a given set of loads $\vec{f}$

The purpose of the study is to describe as precisely as possible all deformed shell configurations like ${}^{1}\Gamma$ and Γ for given sets of loading, prescribed displacements, boundary conditions..... The description includes deformational aspects (displacements for ${}^{0}\Gamma$, rotations, strains) and mechanical aspects (true stresses at the material points).

Two Lagrangian formulations are considered in this report:

- The Total Lagrangian Formulation (TLF). In this case <u>all</u> quantities (displacements, strains and stresses) in the computational process are related to the undeformed initial configuration. The intermediate configurations ${}^{1}\Gamma$ can then be interpreted as final configurations for different sets of loads or prescribed displacements. To obtain the exact Γ solution for thin shells under Kirchhoff's assumption, the nonlinear Green-Lagrange strain - displacement expressions must be complete (no terms neglected). These complete expressions are very complicated and imply second

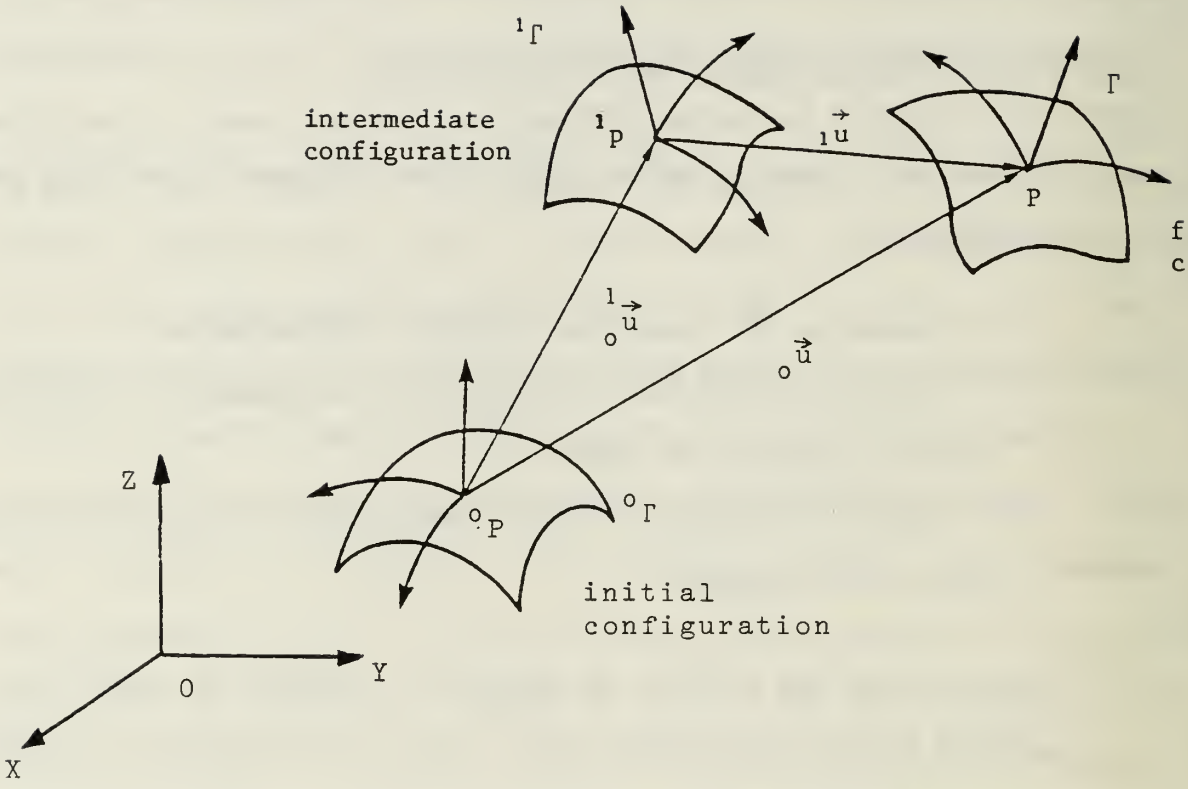

Figure 1 Configurations ${}^{o}\Gamma$, ${}^{1}\Gamma$ and Γ of a Shell Surface

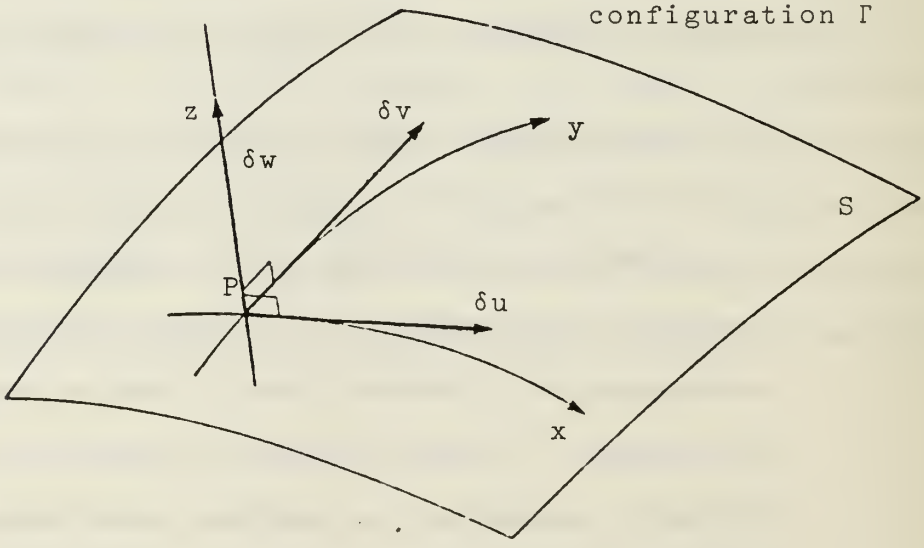

Figure 2 Coordinate Directions x,y,z

derivatives of all the components of the displacement vector $\vec{u}$. Therefore, this approach has not been retained for practical nonlinear analysis unless further assumptions (like the moderate rotation hypothesis) are made.

- The Updated Lagrangian Formulation (ULF). In this case an intermediate configuration ${}^1\Gamma$ is used as a reference configuration to obtain the (final) configuration Γ for a given set of parameters (loads, ...). The ${}^1\Gamma$ configuration is supposed to be known (${}^1\Gamma$ is in fact a previous Γ configuration). That is, ${}^1\Gamma$ can be fully described both from the point of view of geometry and of mechanics (internal stress field). There is theoretically no difference between TLF and ULF (they both want to solve the same equilibrium problem) that is to find Γ. But practically we can take advantage of the fact that ${}^1\Gamma$ is known and that we want to obtain a configuration Γ "not too far" from ${}^1\Gamma$. In ULF, Γ is a neighboring configuration of ${}^1\Gamma$. Hence, we can consider approximate nonlinear strain displacement relations instead of the complicated exact ones to describe Γ from ${}^1\Gamma$. This approach has been considered by many authors for the nonlinear analysis of thin shells [20], [9], [2], [21].

2.2 The principle of virtual work

We consider the equilibrium of a thin shell structure in configuration Γ subjected to body forces $\vec{f}$ only. The internal stresses are described by $\{ \sigma \}$ which is a vector of three components only, under the assumption of plane stress (and neglecting the influence of transverse shear deformation). The conditions of equilibrium in ${}^{*}\Gamma$ leads to the following expression of the principle of virtual work:

$$\Psi = \int_V < \delta e > \{ \sigma \} \, d v - \int_V < \delta u > \{ \overline{f} \} \, d v = 0 \qquad (1)$$

for any $\{ \delta u \}$ such that:

$\{ \delta u \} = \{ 0 \}$ on S_u;

v is the volume in Γ,

S_u is the surface with prescribed displacement,

$\{ \delta u \}$ is an arbitrary virtual displacement vector which is kinematically admissible,

$\{ \delta e \}$ is a virtual strain displacement vector compatible with $\{ \delta u \}$.

We note that the components of $\{ \delta u \}$ are defined with respect to the tangent and normal reference axes of the shell.

The 3D virtual displacement field is of the form:

$$\{ \delta u \} = \{ \delta u_m \} + z \{ \delta \theta \} \qquad (2)$$

z is the coordinate along the thickness h such that:

$$- \frac{h}{2} \leq z \leq + \frac{h}{2} \qquad (3)$$

$\{ \delta u_m \}$ are virtual displacements along two tangent directions x, y on the deformed middle surface S and along the normal of S (Fig. 2). The

first two components of $\{ \delta \theta \}$ are the virtual rotations around axes tangents in S. The third component of $\{ \delta \Theta \}$ is zero:

$$\{ \delta u_m \} = \begin{Bmatrix} \delta u \\ \delta v \\ \delta w \end{Bmatrix} \; ; \quad \{ \delta \theta \} = - \begin{Bmatrix} \delta w,_x \\ \delta w,_y \\ 0 \end{Bmatrix}$$

Expression (2) is compatible with the so called Kirchhoff hypothesis ("normal remains mormal"). Eqs. 1 to 3 after integration through the thickness give:

$$\Psi = \int_S (< \delta u_m > \{ N \} + < \underset{v}{\delta} \kappa > \{ M \}) \, d$$

$$- \int_S (< \delta u_m > \{ \bar{f}_m \} + < \delta \theta > \{ \bar{m} \}) \, d s = 0 \qquad (4)$$

where:

$\{ N \}$ is the three components vector of membrane (direct) forces

$\{ M \}$ is the three components vector of bending moments

$\{ \delta e_m \}$ is the three components vector of virtual membrane strains

$\{ \delta x \}$ is the three components vector of virtual curvatures

$\{ \bar{f}_m \}$ are distributed forces along the tangent directions x, y and along the normal z

$$\{ \bar{f}_m \} = \begin{Bmatrix} f_x \\ f_y \\ f_z \end{Bmatrix} \qquad (5)$$

$\{ \bar{m} \}$ is a two component vector of distributed bending moments acting on the shell surface. (In general these components are zero.)

We note that expression 4 is very general and valid for any curved shell surface where x and y are not necessary orthogonal curvilinear

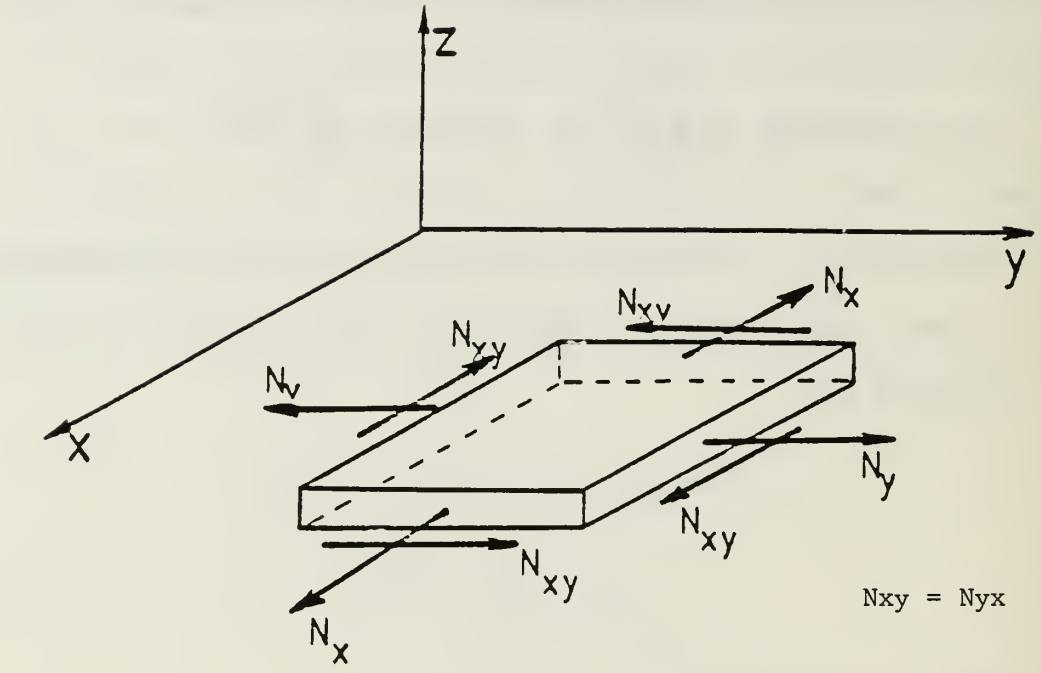

a) membrane forces

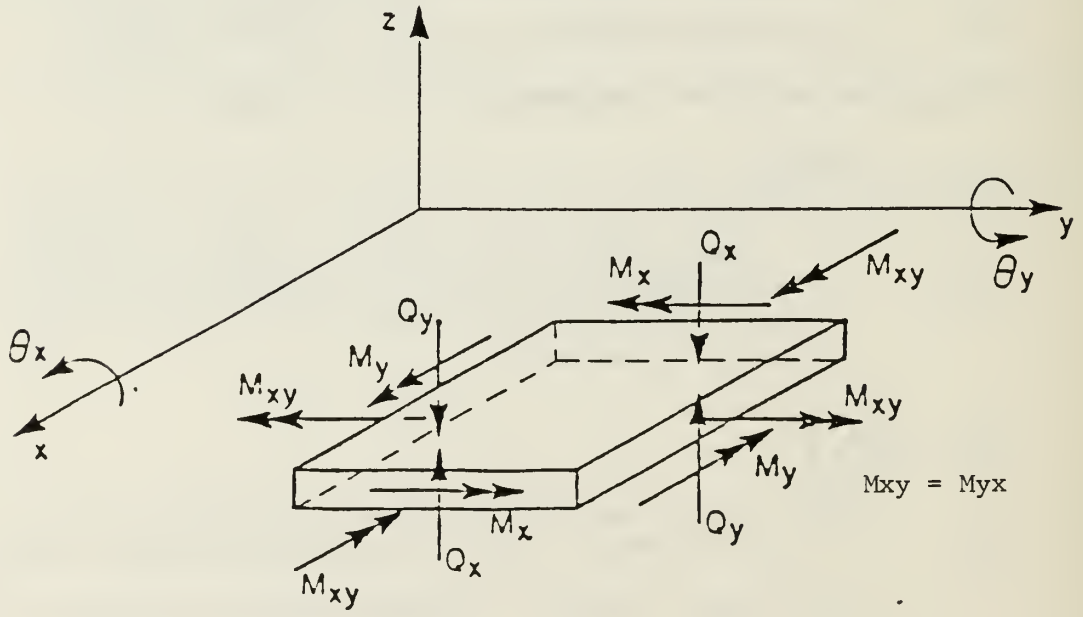

b) bending moments

Figure 3. Shell stress resultants

coordinates. In the case of arbitrary curvilinear coordinates all expressions must be expressed in tensorial notation (with covariant and contravariant quantities).

$\{ \delta e_m \}$ and $\{ \delta \kappa \}$ are expressions in terms of $\{ \delta u_m \}$ and of the curvatures of the middle surface ($\{ \delta \kappa \}$ is an expression of the second derivative of δw).

The positive components of $\{ N \}$ and $\{ M \}$ are given for an orthogonal coordinate system on Figure 3.

The stress resultants are related with the stresses by:

$$\{ N \} = \int_{-\frac{h}{2}}^{\frac{h}{2}} \{ \sigma \} \, dz \; ; \; \{ M \} = \int_{-\frac{h}{2}}^{\frac{h}{2}} \{ \sigma \} \, z \, dz \tag{6}$$

The Euler-Lagrange expressions associated with the variational principle (Eq. 4) are the exact shell equilibrium equations and the mechanical boundary conditions in terms of the stress resultants. These equations are complicated, with coupling between $\{ N \}$ and $\{ M \}$ if the shell is described with arbitrary curvilinear coordinates.

If the shell is flat (or considered so) the three equilibrium equations are the classical ones:

$$\begin{aligned} N_{x,x} + N_{xy,y} + \bar{f}_x &= 0 \\ N_{xy,x} + N_{y,y} + \bar{f}_y &= 0 \\ M_{x,xx} + 2M_{xy,xy} + M_{y,yy} + \bar{f}_z &= 0 \end{aligned} \tag{7}$$

Other expressions of the principle of virtual work (Eq. 1 or 7) can be defined using other reference configuration than Γ: the TLF involves ${}^{0}\Gamma$ and ULF involves ${}^{1}\Gamma$.

2.3 The Total Lagrangian Formulation

2.3.1 General expressions

If we consider the arbitrary displacement field in Eq. 1 as the variation of the displacement field $\overset{\rightarrow}{{}^{\circ}u}$ between ${}^{\circ}\Gamma$ and Γ:

$$\{ \delta u \} \equiv \delta \{ {}_{\circ}u \} = \{ \delta {}_{\circ}u \}$$

then Eq. 1 becomes:

$$\Psi = \int_V < \delta_{\circ} e > \{ \sigma \} dv - \int_V < \delta_{\circ} u > \{ \overline{f} \} dv = 0 \qquad V \{ \delta_{\circ} u \} = \{ 0 \} \text{ on } S_u \tag{8}$$

where the components of $\{ \delta {}_{\circ}u \}$ can be defined with respect to the deformed (unknown) coordinates x, y, z of Γ or with respect to the coordinates ${}^{\circ}x$, ${}^{\circ}y$, ${}^{\circ}z$ in ${}^{\circ}\Gamma$.

Eq. 8 can be modified as:

$$\Psi = \int_{{}^{\circ}V} < \delta_{\circ} \varepsilon > \{ {}_{\circ}S \} d{}^{\circ}v - \int_{{}^{\circ}V} < \delta_{\circ} u > \{ {}_{\circ}\overline{f} \} d{}^{\circ}v = 0 \tag{9}$$

where $\{ {}_{\circ}S \}$ are the components of 2nd Piola - Kirchhoff (P.K.) stresses (tensor $[{}_{\circ}S]$) and $\{ \delta_{\circ} \varepsilon \}$ are the variation of the Green-Lagrange strains (tensor $[{}_{\circ}\varepsilon]$). [3]

We have the following relations:

$$\{ {}_{\circ}\overline{f} \} = {}_{\circ}J \{ \overline{f} \} \tag{10}$$

$$[{}_{\circ}S] = {}_{\circ}J [{}_{\circ}U]^{-1} [\sigma] [{}_{\circ}u]^{-T} \tag{11}$$

$$[\delta_{\circ} \varepsilon] = [\delta_{\circ} U]^{T} [{}_{\circ}U] \tag{12}$$

$J_{\circ}$ is the Jacobian of the deformation, i.e.:

$$J_{\circ} = \frac{dv}{d{}^{\circ}v} = \det [{}_{\circ}F] = \det [{}_{\circ}U] \tag{13}$$

where $[{}^{\circ}F]$ is the deformation gradient at a point of the shell.

$[\ {}_{\circ}F\ ]$ can be decomposed as:

$$[\ {}_{\circ}F\ ] = [\ {}_{\circ}R\ ]\ [\ {}_{\circ}U\ ] \tag{14}$$

where $[\ {}_{\circ}R\ ]$ corresponds to a pure rotation between a set of coordinates in ${}^{\circ}\Gamma$ and the deformed coordinates in Γ (attached at the same material point). $[\ {}_{\circ}U\ ]$ is the symmetic stretch matrix for the material point.

The Green-Lagrange (G-L) strains are:

$$2[\ {}_{\circ}\varepsilon\ ] = [\ {}_{\circ}F\ ]^{T}\ [\ {}_{\circ}F\ ] - [\ I\ ] = [\ {}_{\circ}U\ ]^{T}\ [\ U\ ] - [\ I\ ] \tag{15}$$

since $[\ {}_{\circ}R\ ]$ is orthogonal.

The components of $[\ {}_{\circ}\varepsilon\ ]$ are quadratic expressions in terms of the component displacement of $\overset{\rightarrow}{{}_{\circ}u}$ with respect to the coordinates ${}_{\circ}x,\ {}_{\circ}y,\ {}_{\circ}z$ of ${}^{\circ}\Gamma$. They are invariant with respect to rigid body motion.

Eqs. 11, 13 and 15 show that under the assumption of small strains we have:

$$[\ {}_{\circ}S\ ] \simeq [\ \sigma\ ] \tag{16}$$

$$ {}_{\circ}J \simeq 1 \text{ or } d{}_{\circ}V \simeq dV \tag{17}$$

Eq. 16 means that with the approximation of small strain the 2nd P-K stresses which are work conjugate to the Green-Lagrange strains, corresponds to the "true" Cauchy stresses in the deformed shell. The 2nd P-K stress is therefore a material or co-rotational stress.

This important result is valid for arbitrarily large rotations of the shell and will be used for both the TLF and ULF formulation.

Eqs. 8, 9 and 16 show also that:

$$\{\ \delta_{\circ}\varepsilon\ \} \simeq \{\ \delta_{\circ}e\ \} \tag{18}$$

Equation 9 is an expression of terms of the displacements $\overset{\rightarrow}{{}_{\circ}u}$ and of the coordinates $^{\circ}x$, $^{\circ}y$ and $^{\circ}z$ of $^{\circ}\Gamma$.

2.3.2. Finite element discretization

We consider a shell structure in its initial position $^{\circ}\Gamma$. This shell will be discretized by finite elements (an example using flat faceted triangular and quadrilateral shell elements is presented on Figure 4).

Eq. 9 gives with Eqs. 16 and 17:

$$\Psi = \sum_{e} \left(\int_{v^e} < \delta_{\circ}\varepsilon > \{ \sigma \}\, dv^e - \int_{v^e} < \delta_{\circ}u > \{ \overline{f} \}\, d\, v^e = 0 \right) \tag{19}$$

where $dV^e = d_{\circ}V^e$ represents the elementary volume on a given element e.

If the nodal variables on an element are $\{ {}_{\circ}u_n \}$, than we can write:

$$\{ {}_{\circ}\varepsilon \} = [{}_{\circ}B] \{ {}_{\circ}u_n \} \tag{20}$$

$$\{ \delta_{\circ}\varepsilon \} = [{}_{\circ}B\delta] \{ \delta_{\circ}u_n \} \tag{21}$$

where $[{}_{\circ}B]$ and $[{}_{\circ}B\delta]$ both depend upon $\{ {}_{\circ}u_n \}$

Eqs. 19 to 21 give:

$$\Psi = - \sum_{e} < \delta_{\circ}u_n > \{ {}_{\circ}r_n \} = 0 \tag{22}$$

with

$$\{ {}_{\circ}r_n \} = \{ {}_{\circ}f_{ext} \} - \{ {}_{\circ}f_{int} \} \tag{23}$$

$$\{ {}_{\circ}f_{int} \} = \int_{v^e} [{}_{\circ}B\delta]^T \{ \sigma \}\, d\, v^e \tag{24}$$

$$\int_{v} < \delta_{\circ}u > \{ \overline{f} \}\, dv = < \delta_{\circ}u_n > \{ {}_{\circ}f_{ext} \} \tag{25}$$

After assemblage of all the elements:

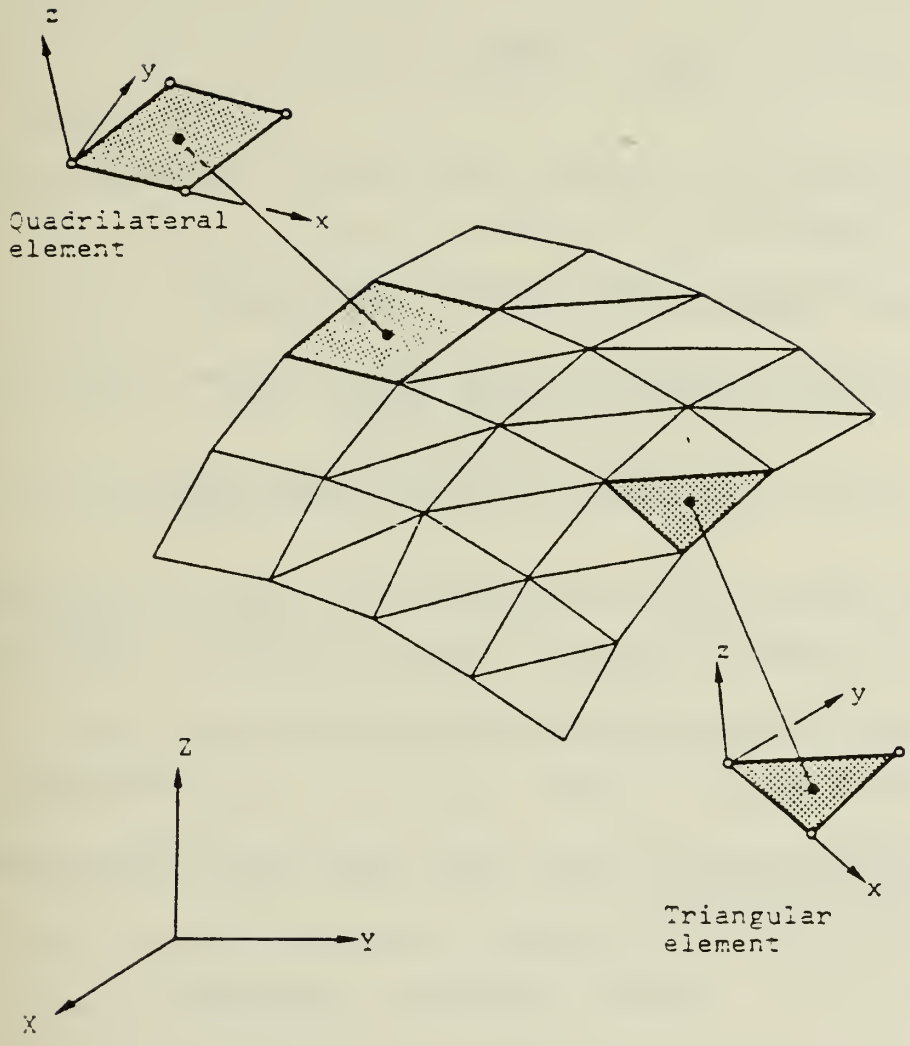

Figure 4 A Shell discretized in Triangular and Quadrilateral Flat elements (from 20)

$$\Psi = - < \delta_o U_n > \{ {}_oR \} = 0 \qquad (26)$$

$$\text{for all } \{ \delta_o U_n \} = \{ 0 \} \text{ on } S_u$$

leading to:

$$\{ {}_oR \} = \{ {}_oF_{ext} \} - \{ {}_oF_{int} \} = \{ 0 \} \qquad (27)$$

$\{ {}_oU_n \}$ is the vector of global nodal variables (displacements between ${}^o\Gamma$ and Γ).

$\{ {}_oR ({}_oU_n) \}$ is the so called residual global vector.

$\{ {}_oF_{ext} ({}_oU_n) \}$ is the vector of the global external forces that may be path-deformation dependant.

$\{ {}_oF_{int} ({}_oU_n) \}$ is the vector of global internal forces.

A solution vector $({}_oU_n \}$ is such that $\{ {}_oR ({}_oU_n) \} = \{ 0 \}$ which represents a system of nonlinear algebraic equations. These equations will be solved using algorithms and strategies based on the Newton-Raphson method. We need, therefore, to define a Jacobian or tangent stiffness matrix $[{}_oK_T]$ which results from the assemblage of element $[{}_ok_T]$ matrices.

A symmetic $[{}_ok_T]$ matrix is defined by considering:

$$\delta \Psi^e = \int_{v^e} (< \delta_o \varepsilon > \{ \delta \sigma \} + < \delta_o^2 \varepsilon > \{ \sigma \} - < \delta_o u > \{ \bar{\delta f} \}) \, d \, v^e \qquad (28)$$

The first term can in general be expressed as:

$$I_1 = < \delta_o u_n > ([{}_ok_\ell] + [{}_ok_{n\ell}]) \{ \delta_o u_n \} \qquad (29)$$

The second term is

$$I_2 = < \delta_o u_n > [{}_ok_\sigma] \{ \delta_o u_n \} \qquad (30)$$

The third term is:

$$I_3 = \langle \delta_o u_n \rangle ([\ {}_o k_\lambda\ ]\ \{\ \delta_o u_n\ \} \tag{31}$$

So that we have:

$$\delta\Psi = \langle \delta_o u_n \rangle [\ {}_o k_t\ ]\ \{\delta_o u_n\ \} \tag{32}$$

with

$$[\ {}_o k_t\ ] = [\ {}_o k \ell\ ] + [\ {}_o k_n \ell\ ] + [\ {}_o k_\sigma\ ] - [\ {}_o k_\lambda\ ] \tag{33}$$

$[\ {}_o k \ell\ ]$ depends only on $\{\ {}_o u_n\ \}$ if the material is nonlinear.

$[\ {}_o k \sigma\ ]$ is the so called geometric stiffness matrix of the form

$$[\ {}_o k \sigma\ ] = \int_{s^e} [\ B\phi\ ]^T [\ N\ ] [\ B\ \phi\ ]\ dS \tag{34}$$

where $[\ B\ \phi\ ]$ is constant in $\{\ {}_o u_n\ \}$ and $[\ N\ ]$ is a 2 by 2 matrix of membrane forces.

$[\ {}_o k_\lambda\ ]$ exists if the loading is path dependant (the case of hydrostatic pressure).

In section 3 the above matrix quantities are discussed for a triangular flat faceted shell element within the approximation of small strains and moderate rotations.

2.4 The Updated Lagrangian Formulation

2.4.1 General expressions

We assume now that an intermediate configuration ${}^1\Gamma$ is obtained (we then know all the quantities regarding geometry as well as internal stresses). (The internal stresses in ${}^1\Gamma$ $\{ {}^1_1\sigma \}$ are in equilibrium with the body forces $\{ {}^1_1\overline{f} \}$.)

We consider again Eq. 1 expressing the equilibrium in Γ with:

$$\{ \delta u \} \equiv \delta \{ {}_1u \} = \{ \delta_1 u \} \tag{35}$$

where $\{ {}_1u \}$ are the displacement components from ${}^1\Gamma$ to Γ. Hence we have:

$$\psi = \int_v < \delta_1 e > \{ \sigma \} \, dv - \int_v < \delta_1 u > \{ \overline{f} \} \, dv = 0$$
$$V \{ \delta_1 u \} = \{ 0 \} \text{ on } S_u \tag{36}$$

Eq. 8 is expressed in terms of 2nd P-K stresses with reference to ${}^1\Gamma$ and variation of Green-Lagrange strain between ${}^1\Gamma$ and Γ:

$$\psi = \int_{{}^1v} < \delta_1 \varepsilon > \{ {}^1_1S \} \, d^1v - \int_{{}^1v} < \delta_1 u > \{ {}^1_1\overline{f} \} \, d^1v = 0 \tag{37}$$

with

$$\{ {}_1\overline{f} \} = {}_1J \{ \overline{f} \} \tag{38}$$

$$\{ {}_1S \} = {}_1J [{}_1U]^{-1} [\sigma] [{}_1U]^{-T} \tag{39}$$

$$\{ \delta_1 \varepsilon \} = [\delta_1 U]^T [{}_1U] \tag{40}$$

$${}_1J = \frac{d\,V}{d^1V} = \det [{}_1F] = \det [{}_1U] \tag{41}$$

$$[\ {}_1F\ ] = [\ {}_1R\ ]\ [\ {}_1U\ ] \tag{42}$$

$$2\ [\ {}_1\varepsilon\ ] = [\ {}_1F\ ]^T\ [\ {}_1F\ ] - [\ I\ ] = [\ {}_1U\ ]^T\ [\ {}_1U\ ] - [\ I\ ] \tag{43}$$

With the approximation of small strains (section 3.1) Eq. 36 can be replaced by:

$$\psi = \int_V < \delta_1\varepsilon > \{\ \sigma\ }\ dv - \int_V < \delta_1 u > \{\ \overline{f}\ }\ dv = 0$$
$$V\ \{\ \delta_1 u\ } = \{\ 0\ } \text{ on } S_u \tag{44}$$

with

$$\{\ \sigma\ } = \{\ {}^1_1\sigma\ } + \{\ {}_1\sigma\ }$$
$$\{\ \overline{f}\ } = \{\ {}^1\overline{f}\ } + \{\ {}_1\overline{f}\ } \tag{45}$$

where $\{\ {}_1\sigma\ }$ are the incremental stresses between ${}^1\Gamma$ and Γ and $\{\ {}_1\overline{f}\ }$ the incremental forces between ${}^1\Gamma$ and Γ.

In Eq. 44 $\{\ \delta_1\varepsilon\ }$ are dependent upon the variations of the displacements between ${}^1\Gamma$ and Γ and not upon the displacements $\{\ {}^1_o u\ }$.

In general ${}^1\Gamma$ is a curved surface and the exact expressions of $[\ {}_1\varepsilon\ ]$ are not simpler than $[\ {}_o\varepsilon\ ]$. In fact they are theorically identical when the lower left index o is replaced by index 1.

2.4.2 Finite Element discretization

The shell in configuration ${}^{1}\Gamma$ is discretized by finite elements. The finite element matrices are of the same general nature as for the TLF. We just have to substitute index o with index 1.

In defining the tangent stiffness matrix $[\ {}_{1}k_{t}\ ]$ by considering $\delta\Psi^{e}$ we simply have to take account of the fact that:

$$\{\ \delta\sigma\ \} = \{\ \delta_{1}\sigma\ \}$$

and $$\{\ \delta\overline{f}\ \} = \{\ \delta_{1}\overline{f}\ \}$$

In the ULF the "solution" means to find the displacements and the additional stresses between ${}^{1}\Gamma$ and Γ that are such that:

$$\{\ {}_{1}R\ \} = \{\ {}_{1}f_{ext}\ \} - \{\ {}_{1}f_{int}\ \} = \{\ 0\ \} \qquad (46)$$

3. DESCRIPTION OF A FLAT TRIANGULAR SHELL ELEMENT

3.1 The DKT18 shell element for linear elastic shells.

The nonlinear analysis presented in this report is based on the discretization of shells by flat triangular shell elements having three nodes and the six engineering d.o.f. per node (Fig. 5):

$$\begin{aligned} < u_n > = < & U_1 \quad V_1 \quad W_1 \quad RX_1 \quad RY_1 \quad RZ_1 \\ & U_2 \quad V_2 \quad W_2 \quad RX_2 \quad RY_2 \quad RZ_2 \\ & U_3 \quad V_3 \quad W_3 \quad RX_3 \quad RY_3 \quad RZ_3 > \end{aligned} \tag{47}$$

U_i, V_i, W_i $i = 1,3$ are the translational d.o.f with respect to the global coordinates axes X, Y, Z.

RX_i, RY_i, RZ_i $i = 1,3$ are the rotational d.o.f. around the global axis X, Y, Z.

The DKT18 element results from the superposition of the low order membrane constant strain triangular element CST with 6 d.o.f. and of the efficient bending triangular element DKT having 9 d.o.f. (Fig. 6).

The linear stiffness matrix of a DKT18 shell element can be expressed with respect to the local d.o.f.:

$$\begin{aligned} < \underset{\sim}{u}_n > = < & u_1 \quad v_1 \quad w_1 \quad \theta_{x1} \quad \theta_{y1} \quad \theta_{z1} \\ & u_2 \quad v_2 \quad w_2 \quad \theta_{x2} \quad \theta_{y2} \quad \theta_{z2} \\ & u_3 \quad v_3 \quad w_3 \quad \theta_{x3} \quad \theta_{y3} \quad \theta_{z3} > \end{aligned} \tag{48}$$

as [22]; [11]:

$$[\, \underset{\sim}{k}_\ell \,] = [\, \underset{\sim}{k}_m \,] + [\, \underset{\sim}{k}_b \,] + [\, \underset{\sim}{k}_{\theta z} \,] \tag{49}$$

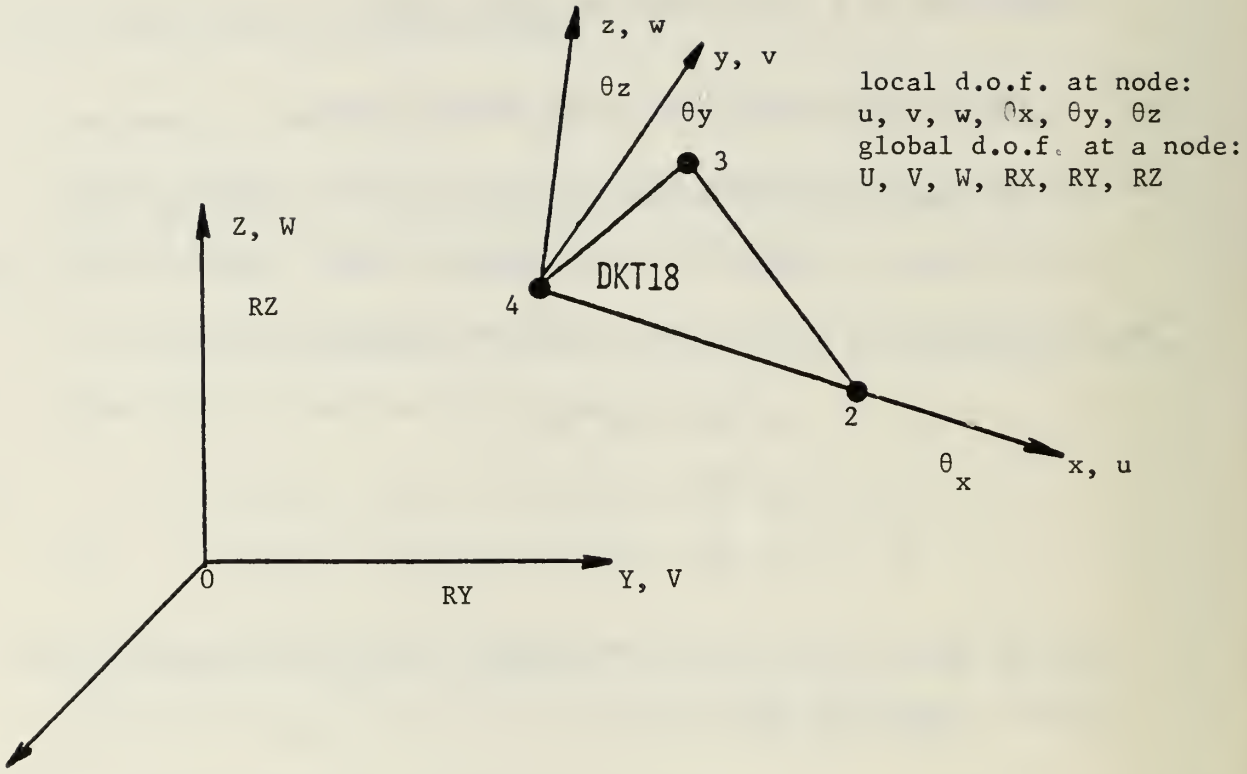

Figure 5. DKT18 Shell element

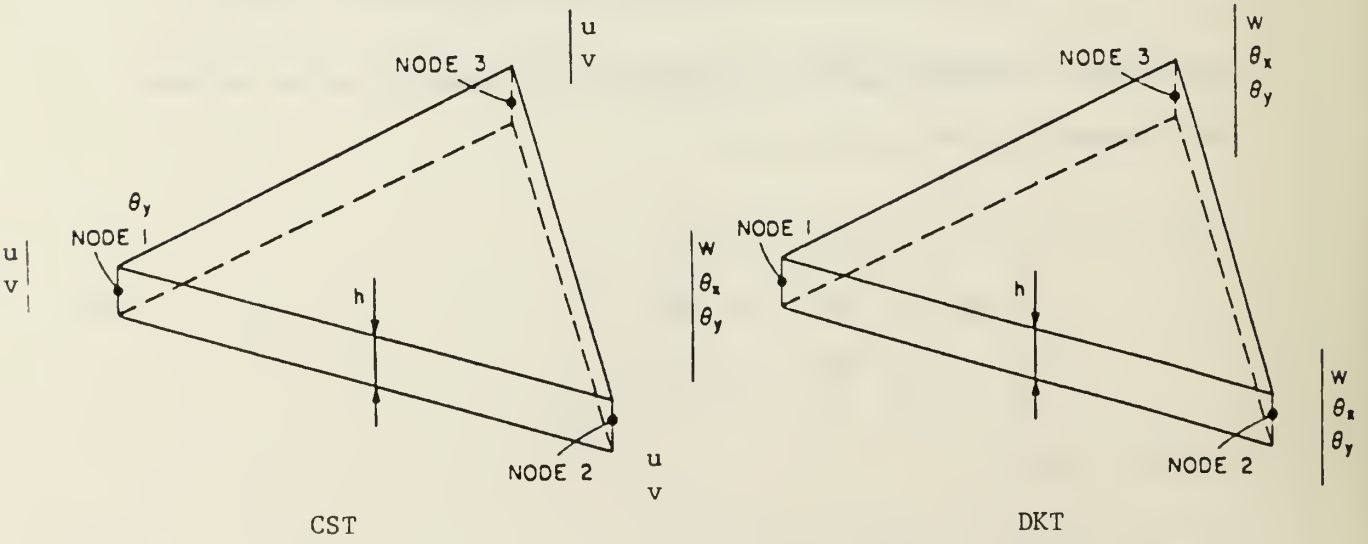

Figure 6. CST and DKT plate elements

[$\underset{\sim}{k}_m$] is the stiffness matrix of the CST element. It is a simple matrix with constant terms. No numerical integration is necessary since the displacement u and v are linear.

[$\underset{\sim}{k}_b$] is the stiffness matrix of the 9 d.o.f. DKT plate bending element. This element is well documented in [6], [7], [8] and is obtained from the the technique of discrete Kirchhoff constraints. This simple plate bending element satisfies all convergence criteria (like the patch-tests) and has been found very effective and reliable for thin plate bending analysis. It has shown good behavior with respect to element distortions. The stiffness matrix of the DKT element is obtained exactly (in linear analysis) with 3 numerical integration points in the elements [19].

[$\underset{\sim}{k}_{\theta Z}$] is a fictitious stiffness matrix with non-zero components related to θ_{Z1}, θ_{Z2}, θ_{Z3} only. This matrix is necessary in order to avoid the singularity of the stiffness matrix in the case of coplanar elements. The coefficients of this matrix should be small enough so that they do not modify the correct solution (with membrane and bending energy only) and big enough to avoid numerical errors. Two approaches are considered. The first is described in [23, Eq. 13.18] with $\alpha = 10^{-4}$ for our computations on double precision VAX computers. The second method is to consider only diagonal coefficients with values α times the minimum of the diagonal rotational coefficients of the bending stiffness matrix. [10]

In the case of symmetrical material properties with respect to the middle surface of the shell the stiffness matrices [$\underset{\sim}{k}_m$], [$\underset{\sim}{k}_f$], [$\underset{\sim}{k}_{\theta z}$] are not coupled so that a large number of coefficients of [k_ℓ] are zeros.

The local coordinate x, y, z of an element are shown on Fig. 5. x axes coincides with side 1-2 (origin in 1) z is normal to the plane 123 (with direction resulting from the cross products of $\vec{12} \times \vec{13}$). y is such that x, y, z are orthogonal and right-handed. The relation between the local coordinates and the global ones are [22], [23];

$$\{ x \} = [\lambda] \{ X \} \tag{50}$$

with

$$\begin{aligned} < x > &= < x, y, z > \\ < X > &= < X, Y, Z > \end{aligned} \tag{51}$$

$[\lambda]$ is a 3 by 3 matrix of the direction cosines of x, y, z with respect to X, Y, Z.

The element local d.o.f. $\{ \underset{\sim}{u}_n \}$ are related to the global ones $\{ u_n \}$ by:

$$\{ \underset{\sim}{u}_n \} = [T] \{ u_n \} \tag{52}$$

with

$$[T] = \begin{bmatrix} [\lambda] & 0 \\ & \\ 0 & [\lambda] \end{bmatrix} \tag{53}$$

Therefore, the stiffness matrix of a shell element in the global coordinate system is:

$$[k_\ell] = [T]^T [\underset{\sim}{k}_\ell] [T] \tag{54}$$

If $[\underset{\sim}{f}_\ell]$ is a force vector resulting from the discretization of

distributed loads on the elements (components $\overline{f}_x$, $\overline{f}_y$ or $\overline{f}_z$) then the corresponding force vector in the global coordinate system is:

$$\{ f \} = [T]^T \{ \underset{\sim}{f} \} \tag{55}$$

After the process of assemblage, modification due to boundary conditions and solution of the linear system we can obtain the strains and the stresses at any point in the element:

$$\{ \varepsilon_\ell \} = [B_m] \{ \underset{\sim}{u}_n^m \} + z [B_b] \{ \underset{\sim}{u}_n^f \} \tag{56}$$

where

$$\begin{aligned} \langle \underset{\sim}{u}_n^m \rangle &= \langle u_1 \quad v_1 \quad u_2 \quad v_2 \quad u_3 \quad v_3 \rangle \\ \langle \underset{\sim}{u}_n^b \rangle &= \langle w_1 \quad \theta_{x1} \quad \theta_{y1} \quad w_2 \quad \theta_{x2} \quad \theta_{y2} \quad w_3 \quad \theta_{x3} \quad \theta_{y3} \rangle \end{aligned} \tag{57}$$

$[B_m]$ is constant and $[B_b]$ (the linear strain operator of the DKT plate element) is linear in x, y.

In the absence of coupling between membrane and bending effects we have:

$$\begin{aligned} \{ N \} &= [D_m] [B_m] \{ \underset{\sim}{u}_n^m \} \\ \{ M \} &= [D_b] [B_b] \{ \underset{\sim}{u}_n^b \} \end{aligned} \tag{58}$$

and therefore:

$$\{ \sigma \} = [D_m] [B_m] \{ \underset{\sim}{u}_n^m \} + z [D_b] [B_b] \{ \underset{\sim}{u}_n^b \} \tag{59}$$

$[D_m]$ and $[D_b]$ are 3 by 3 membrane and bending material matrices. In the ususal case of plane stress isotropic material:

$$[\ D_m\ ] = \frac{Eh}{1-\nu^2}\begin{bmatrix} 1 & \nu & 0 \\ \nu & 1 & 0 \\ 0 & 0 & \frac{1-\nu}{2} \end{bmatrix};\quad [\ D_b\ ] = \frac{h^2}{12}\ [\ D_m\ ] \tag{60}$$

where E and ν are Young's modulus and Poisson's ratio.

Eq. 58 shows that in general the membrane forces are constant and the bending moments vary linearly.

We have computed the stress resultants, the principal stresses and the Von Mises equivalent stress on the outer faces of the shell at the maximum of 7 points per element (centroid, integration points, corner nodes). The corner node values are discontinuous but can provide useful information with respect to node location and with respect to precision in the results.

The simple DKT18 shell elements has been used extensively for linear analysis of shells and is implemented in several computer codes working on mini and micro-computers. The main disadvantage of the element are the CST element as membrane element and sometimes the non-energy associated θ_Z d.o.f.'s.

3.2 The element matrices for TLF nonlinear analysis

Our TLF combined with the use of the flat triangular DKT18 shell element is based on the following definition of the G-L strain:

$$\{ {}_{o}\varepsilon \} = \{ \varepsilon_{\ell} \} + \{ \varepsilon_{n\ell} \} \tag{61}$$

with

$$\{ \varepsilon_{\ell} \} = \begin{Bmatrix} u,_x & + z\ \theta_y,_x \\ v,_y & - z\ \theta_x,_y \\ u,_y + v,_x & - z\ \theta_x,_x - \theta_y,_y \end{Bmatrix} \tag{62}$$

$$\{ \varepsilon_{n\ell} \} = \begin{Bmatrix} \frac{1}{2} & w,_x^2 \\ \frac{1}{2} & w,_y^2 \\ w,_x & w,_y \end{Bmatrix} \tag{63}$$

where the lower left index o has been omitted everywhere for simplification, i.e., u, v, w, θ_x and θ_y are displacements and rotations with respect to axes x, y, z of the undeformed shell element.

$\{ \varepsilon_{\ell} \}$ is the vector of linear strains which leads to the linear stiffness matrices $[\underset{\sim}{k}_m]$ and $[\underset{\sim}{k}_b]$ presented in section 3.1.

$\{ \varepsilon_{n\ell} \}$ involves only derivative of w with respect to x and y. This nonlinear part of G-L strain is associated with the so-called Von Karman plate theory, that is this expression, will be valid only for large displacements and moderate rotations. Therefore, the TLF discussed here is valid with the above assumption and a flat triangular discretization of the shell in its initial configuration.

Eq. 61 gives:

$$\{ \delta_o \varepsilon \} = [B\delta] \{ \delta \underset{\sim}{u}_n \} \tag{64}$$

where $< \delta \underset{\sim}{u}_n > = \delta < \underset{\sim}{u}_n >$

with $< \underset{\sim}{u}_n >$ given in Eq. 48.

$$[B_\delta] = [B_\ell] + [B_{n\ell}] \tag{65}$$

$[B_\ell]$ is the linear operator which leads to $[\underset{\sim}{k}_m]$ and $[\underset{\sim}{k}_b]$

$$[B_{n\ell}] = \begin{bmatrix} w,x & < N^w_{,x} > \\ w,y & < N^w_{,y} > \\ w,y & < N^w_{,x} > + w_{1x} < N^w_{,y} > \end{bmatrix} \tag{66}$$

with

$$w = < N^w > \{ \underset{\sim}{u}_n \} \tag{67}$$

$< N^w >$ has nine non zero components which are associated with a cubic Hermite interpolation function for w. This 9 term interpolation function is chosen so that it is invariant with respect to local coordinate x, y. This incomplete cubic interpolation is given in [23, Eq. 10.29].
The internal forces Eq. 24 for the element in the global coordinate system is then defined as :

$$\{ {}_\circ f_{int} \} = [{}_\circ T]^T \int_{v^e} [B\delta]^T \{ \sigma \} dV^e \tag{68}$$

with $[{}_\circ T] = [T]$ given in Eq. 53 and $[B\delta]$ given in 65 and 66. For the case of elastic behavior:

$$\{ \sigma \} = [D] ([B_\ell] + \frac{1}{2} [B_{n\ell}]) \{ \underset{\sim}{u}_n \} \tag{69}$$

$\{ {}_\circ f_{ext} \}$ Eq. 25 depends on the loading. If the loads are not path dependant $\{ f_{ext} \}$ is constant, if not $\{ f_{ext} \}$ is a function of $\{ \underset{\sim}{u}_n \}$. The interpolation functions for the evaluation of the equivalent forces (Eq. 25) are considered linear for u, v, w.

The following expression can be considered in the case of uniform normal pressure of intensity $\bar{p}$ with respect to the deformed middle surface:

$$\delta W_p = \bar{p} \int_{s^e} (- w,_x \, \delta u - w,_y \, \delta v + \delta w) \, dxdy$$
$$= < \delta \underset{\sim}{u}_n > \{ \underset{\sim}{f}^p_{ext} \} = < \delta u_n > \{ \underset{\sim}{f}^p_{ext} \} \tag{70}$$

with

$$\{ {}_o\underset{\sim}{f}^p_{ext} \} = [T]^T \{ \underset{\sim}{f}^p_{ext} \} \tag{71}$$

The tangent stiffness $[{}_ok_t]$ as defined in Eq. 33 is such that:

$$[{}_ok_t] = [T]^T [{}_o\underset{\sim}{k}_t] [T] \tag{72}$$

where

$$[{}_o\underset{\sim}{k}_t] = [\underset{\sim}{k}_\ell] + [{}_o\underset{\sim}{k}_{n\ell}] + [{}_o\underset{\sim}{k}_\sigma] \tag{73}$$

$[\underset{\sim}{k}_\ell]$ is given in Eq. 49.

For elastic material:

$$\{ \delta\sigma \} = [D] \{ \delta\varepsilon \} \tag{74}$$

Therefore:

$$[{}_o\underset{\sim}{k}_{n\ell}] = \int_{v^e} [B_\ell]^T [D] [B_{n\ell}] + [B_{n\ell}]^T [D] [B_\ell] + [B_{n\ell}]^T [D] [B_{n\ell}] \, dv^e \tag{75}$$

Moreover:

$$[{}_o\underset{\sim}{k}_{n\sigma}] = \int_{s^e} [B_\phi]^T [N] [B_\phi] \, dxdy \tag{76}$$

where

$$[\ N\ ] = \begin{bmatrix} N_x & N_{xy} \\ N_{xy} & N_y \end{bmatrix} \tag{77}$$

$$[\ B\phi\ ] = \begin{bmatrix} < N^w_{,x} > \\ \\ < N^w_{,y} > \end{bmatrix} \tag{78}$$

with $< N^w >$ the 9 term cubic function Eq. 67.

The $[\ k_\lambda\ ]$ matrix is not necessary for our moderate rotation TLF.

Matrices $[\ {}_o\underset{\sim}{k}_{n\ell}\ ]$ and $[\ {}_o\underset{\sim}{k}_\sigma\ ]$ are evaluated with no neglecting terms in the tangent stiffness matrix using 3 numerical integration points.

The TLF as presented above will give the nonlinear solution of arbitrary shell structures within the approximations considered. That is, the converging solution with mesh refinement will always be restricted to the moderate rotation assumptions.

3.3 The element matrices for ULF nonlinear analysis

In our Updated Lagrangian Formulation using the DKT18 shell elements the intermediate configurations ${}^1\Gamma$ are not the exact configurations of the shell. These approximate configurations will result from:

- the discretization of the shell using flat triangular elements
- the assumption of moderate rotations between two configurations (like between ${}^1\Gamma$ and Γ).

Hence the configuration Γ is obtained from ${}^1\Gamma$ by making the same assumptions and the same type of computations as between ${}^\circ\Gamma$ and Γ in the TLF procedure.

So we assume that the current coordinates in ${}^1\Gamma$ are known. They result from:

$$\{ {}^1_\circ x \} = \{ {}_\circ x \} + \{ {}^1_\circ u \} \tag{79}$$

(The curvatures in ${}^1\Gamma$ are neglected as they are in ${}^\circ\Gamma$). We also assume that the Cauchy "true" stresses $\{ {}^1_1\sigma \}$ are obtained (and stored at the integration points of the triangular elements). These stresses are in equilibrium with the surface forces ${}^1_\circ\bar{f}_x$, ${}^1_\circ\bar{f}_y$ and ${}^1_\circ\bar{f}_z$.

The necessary information to obtain Γ are the residual vectors and the tangent matrices of each element. These quantities are obtained in a similar manner as in TLF.

The internal forces $\{ {}_1f_{int} \}$ are defined as:

$$\{ {}_1f_{int} \} = [{}_1T]^T \int_{v^e} [{}_1B\delta]^T \{ \sigma \} dV \tag{80}$$

$[\ {}_1T\ ]$ is the matrix of direction cosines between the local axes ${}^1x$, ${}^1y$, ${}^1z$ in ${}^1\Gamma$ and the global axes X, Y, Z.

$[\ {}_1B\delta\ ]$ is similar to Eqs. 65 and 66 where w is the displacement in the ${}^1z$ direction between ${}^1\Gamma$ and Γ.

$\{\ \sigma\ \}$ is defined as:

$$\{\ \sigma\ \} = \{\ {}^1_1\sigma\ \} + \{\ {}_1\sigma\ \} \tag{81}$$

and

$$\{\ {}_1\sigma\ \} = [\ D\ ]\ ([\ B_\ell\ ] + \frac{1}{2}\ [\ {}_1B_{n\ell}\ ]\ \{\ {}_1u_n\ \} \tag{82}$$

$\{\ {}_1u_n\ \}$ are the nodal d.o.f. in the global coordinate system and refer to displacements and rotations between ${}^1\Gamma$ and Γ.

The external forces $\{\ {}_1f_{ext}\ \}$ include the forces from ${}^\circ\Gamma$ to Γ.

The tangent stiffness matrix is kept complete and is given by:

$$[\ {}_1k_t\ ] = [\ {}_1T\ ]^T\ [\ {}_1\underset{\sim}{k}_t\ ]\ [\ {}_1T\ ] \tag{83}$$

where $[\ {}_1\underset{\sim}{k}_t\ ]$ is similar to $[\ {}_\circ\underset{\sim}{k}_t\ ]$.

We again note that the geometric stiffness matrix $[\ {}_1\underset{\sim}{k}_\sigma\ ]$ contains the influence of the stresses from ${}^\circ\Gamma$ to Γ, and that $[\ {}_1\underset{\sim}{k}_{n\ell}\ ]$ is nonlinear in terms of ${}_1w$ (from ${}^1\Gamma$ to Γ).

We note that the follower forces are easily taken into account in the ULF since the coordinates (and therefore the element orientations) are updated after each new known configuration.

The performance of the ULF in computing with precision the nonlinear response of shells with large rotations will not only depend on the

number of elements but also on the number of steps (or configurations ${}^{1}\Gamma$) between ${}^{\circ}\Gamma$ and the unknown configuration Γ, because of the assumption of moderate rotation between two configurations.

4. ON THE AUTOMATIC SOLUTION FOR PRE AND POST BUCKLING

4.1 Solving the nonlinear equations.

The solution in both TLF and ULF must satisfy a set of simultaneous nonlinear algebraic equations as given by Eq. 27 or 46 of the form:

$$\{ R(U,\lambda) \} = \lambda \{ F_{ext}(U) \} - \{ F_{int} \} = \{ 0 \} \qquad (84)$$

where the number of equations n is equal to the total active d.o.f. of the discretized problem, ($\{ U \}$ stands for these active d.o.f). λ is a load parameter (we consider only one variable loading). $\{ F_{int} \}$ is always a function of $\{ U \}$ and $\{ F_{ext} \}$ is so only if the loading is path dependent.

In the nonlinear analysis of shell structures, the "load-displacement" curves can exhibit all kinds of forms depending on the problem (geometry, loading, boundary conditions, material properties). [1], [2]...

In this report we consider only elastic behavior of shells with large displacements and large rotations, pre and post-buckling with multiple limit points, snap-through and snap-back behavior. The problem of determining Euler bifurcation loads by solving linear eigenvalue problems is not considered although the basic ingredients (stiffness matrices, geometric stiffness matrices, and eigenvalue equation solvers are available). Bifurcation loads can, however, be obtained after the introduction of a perturbing parameter that discloses the bifurcation mode.

The complete determination of the load displacement curves can be performed using different strategies all based on a number of iterative

methods. The problem is to obtain:

- the n components of $\{ U \}$ for a given λ or
- the n components of $\{ U \}$ and λ with one constraint equation.

The over-all behavior of the load-displacement curves can be characterized by the so-called current stiffness parameter [24] Sp.

One simple definition in the case of constant loading is:

$$Sp = \frac{\Delta\lambda^P < \Delta U_\ell > \{ F \}}{\Delta\lambda_\ell < \Delta U^P > \{ F \}} \tag{85}$$

$\{ \Delta U_\ell \}$ is the linear solution for $\Delta\lambda_\ell$. $\{\Delta U^P\}$ and $\Delta\lambda^P$ are the increments of displacements and of load at step p. Sp is a useful parameter in an automatic determination of the complete load displacement curves.

Three strategies have been implemented and used to solve various nonlinear shell problems. The first is the load control strategy (prescribed λ), the second is the one-displacement control strategy (one prescribed component of $\{ U \}$), the third is the arc-length strategy involving all d.o.f..

The three strategies are using the Newton-Raphson method to obtain the incremental solutions and are as automatic as possible within their own limitations.

4.2 The Newton-Raphson method with prescribed forces.

The algorithm is the following [ ], (Fig. 7a):

step p : λ^p, $\{ U^p \}$ known solution

step p+1: $\lambda^{p+1} = \overline{\lambda}$ $\{ U^1 \} = \{ U^p \}$

iterations: i = 1 to NITER

$$\{ R^i \} = \overline{\lambda} \{ F_{ext} (U^i) \} - \{ F_{int} (U^i) \}$$

$$[K_T^i] \{ \Delta U \} = \{ R^i \} \qquad (86)$$

$$\{ U^{i+1} \} = \{ U^i \} + \{ \Delta U \}$$

TEST convergence

step p + 2 ...

where $[K_T^i]$ is the global tangent stiffness matrix which is computed at each iteration in the full Newton-Raphson (N-R) method or computed only at the beginning of the iteration process in the modified N-R method.

The test of convergence is:

$$\text{TEST} < \text{EPSILON} \qquad (87)$$

with TEST defined as:

$$\text{TEST1} = \frac{|| \Delta U ||}{|| U^i ||} \qquad (88)$$

or

$$\text{TEST2} = \frac{|| \Delta U ||}{|| U^i - U^p ||} \qquad (89)$$

where $|| U || = (< U > \{ U \})^{1/2}$ is the Euclidean norm of the total displacement vector. We have usually considered EPSILON = 10^{-3} if TEST1 is used and 10^{-2} if TEST2 is used. The TEST2 is motivated so that all

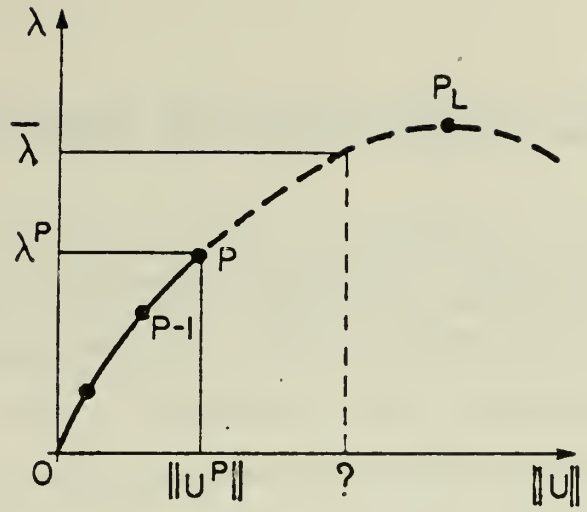

a) prescribed load

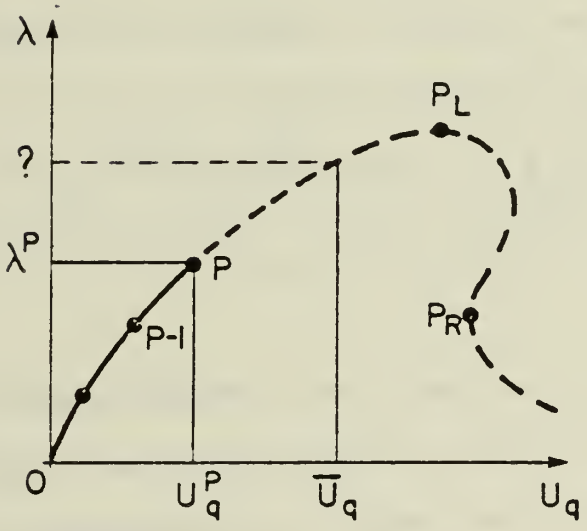

b) prescribed displacement

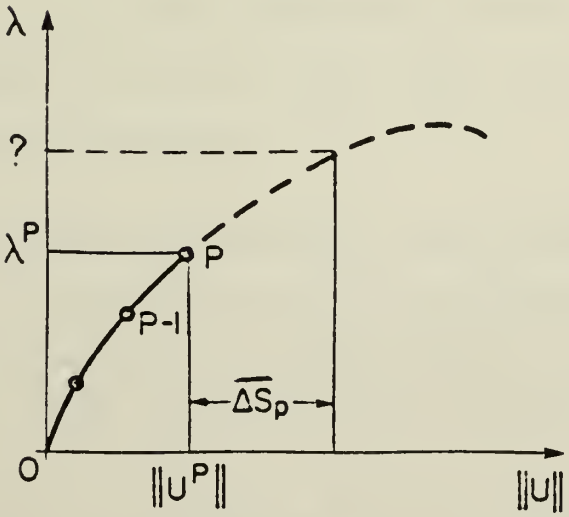

c) prescribed arc-length (or displacement norm)

Figure 7 Nonlinear solution strategies

steps (particularly in the ULF) will have the same convergence requirements.

$\overline{\lambda}$ is fixed by the user or determined automatically. If no convergence has occurred (i.e., i> NITER and TEST > EPSILON) than the given $\overline{\lambda}$ or $\overline{\Delta\lambda}$ is cut by two automatically until convergence is reached. $\overline{\Delta\lambda}_p = \lambda^{p+1} - \lambda^p$ can also be modified depending on the convergence rate and according to:

$$\overline{\Delta\lambda}_p = \overline{\Delta\lambda}_{p-1} \left(\frac{Id}{Ip-1}\right)^{\alpha} \tag{90}$$

where $\overline{\Delta\lambda}_{p-1}$ is the increment of loading at the previous solution step. Id is a number of required iterations and I_{p-1} is the number of iterations at step p-1. α is a number defined by the user. We have considered α = 1 and 0.5 with Id = 4 in the full N-R and 6 in the modified N-R.

The above strategy has been found effective to obtain the load deflection curves automatically up to the first limit point, giving the buckling load, (and therefore the complete nonlinear response if there is no limit point).

4.3 The N-R method with a prescribed displacement component.

This algorithm has been found very efficient to obtain the post-buckling response when a particular component of the displacement vector still increases after the limit load. [12], [13], [25]

The algorithm is the following (Fig. 7b):

step p : λ^p, $\{ U^p \}$ known solution

step p+1 : $\lambda^1 = \lambda^p$; $\{ U^1 \} = \{ U^p \}$

iterations: i = 1 to NITER

$$\{ R^i \} = \lambda^i \{ F_{ext}^i \} - \{ F_{int}^i \}$$

$$[K_T^i] (\{ \Delta U_R \} \quad \{ \Delta U_F \}) = (\{ R^i \} \quad \{ F_{ext}^i \}) \qquad (91)$$

$$\{ U^{i+1} \} = \{ U^i \} + \{ \Delta U_R \} + \Delta\lambda \{ \Delta U_F \}$$

$$\lambda^{i+1} = \lambda^i + \Delta\lambda$$

where $\Delta\lambda$ is such that

$$(\Delta U_R)q + \Delta\lambda (\Delta U_F)q = \Delta\bar{U}q$$

TEST convergence

step p + 2 ...

where $\Delta\bar{U}q$ is a prescribed displacement increment, $(\Delta U_R)q$ and $(\Delta U_F)q$ are the q^{th} component of vectors $\{ \Delta U_R \}$ and $\{ \Delta U_F \}$. It is also possible to use the modified N-R method.

For the same problem and convergence test the above algorithm leads in general to a faster rate of convergence compared to the prescribed loading. This is due to the modification of $[K_T^i]$ after the first iteration. However, two load vectors are considered at each iteration.

As in the previous algorithm, ΔUq can be automatically adjusted if

convergence doesn't occur within the limitation given by the user. This algorithm is very efficient in many snap-through situations and works until a limit point in displacement (snap-back) occurs.

The above algorithm is a particular case of the arc-length algorithm as discussed below.

4.4 The N-R and arc-length control method.

The so-called arc-length or modified arc-length method has received a great attention in the last five years [14], [15], [16], [17], [18], [26].

The algorithm is similar to the previous one (displacement control). It is only different in the evaluation of $\Delta\lambda$ at the first and subsequent iterations. (Fig. 7c):

step p : λ^p, $\{ U^p \}$ known solution

step p+1 : $\lambda^1 = \lambda^p$; $\{ U^1 \} = \{ U^p \}$

iterations: i = 1 to NITER

$$\{ R^i \} = \lambda^i \{ F^i_{ext} \} - \{ F^i_{int} \}$$

$$[K^i_T] (\{ \Delta U_R \} \{ \Delta U_F \}) = \{ R^i \} \{ F^i_{ext} \}) \qquad (92)$$

$$\{ U^{i+1} \} = \{ U^i \} + \{ \Delta U_R \} + \Delta\lambda \{ \Delta U_F \}$$

$$\lambda^{i+1} = \lambda^i + \Delta\lambda$$

where $\Delta\lambda$ is such that

$$< U^{i+1} - U^p > \{ U^{i+1} - U^p \} = (\Delta\bar{S}_p)^2 \qquad (93)$$

and

$$< U^i - U^p > \{ U^{i+1} - U^p \} > 0 \quad i>1$$

$$< U^p - U^{p-1} > \{ U^2 - U^p \} > 0 \quad i=1 \qquad (94\ a,b)$$

TEST convergence

step p + 2 ...

Eq. 93 is a quadratic equation in $\Delta\lambda$ that can be written as:

$$a\ \Delta\lambda^2 + b\ \Delta\lambda + c = 0 \qquad (95)$$

with

$$a = \langle \Delta U_F \rangle \{ \Delta U_F \}$$

$$b = 2 \langle \Delta U_F \rangle \{ V \}$$

$$c = \langle V \rangle \{ V \} - (\overline{\Delta S}_p)^2$$

$$\langle V \rangle = \langle \Delta U_R \rangle + \langle U^i - U^p \rangle$$

If no real root of Eq. 94 exists, the arc-length $\overline{\Delta S}_p$ must be reduced. The choice of the real root is such that Eq. 94a or b is satisfied.

One should mention here that other definitions of the arc-length (Eq. 93) can be made, but the above relation has been found effective to solve our examples.

As in the two other strategies, it is possible to adjust automatically the value of $\overline{\Delta S}_p$ between two steps:

- no convergence $\overline{\Delta S}_p = 0.5 \ \overline{\Delta S}_{p-1}$

- if convergence $\overline{\Delta S}_p = \overline{\Delta S}_{p-1} \left[\frac{Id}{I_{p-1}} \right]^{\alpha}$ (96)

  with Id, I_{p-1}, α as discussed in section 4.2.

If the arc-length strategy is used, we first start the problem using one of the two previous methods (load or displacement method). Then we compute $\overline{\Delta S}_2$ using Eq. 93 to obtain the solution at step 2 using the arc-length algorithm.

5. NUMERICAL RESULTS

5.1 Comments on the computational procedure

A FORTRAN program has been written partly for this research. The basic routines of the finite element method are those documented in [19]. We have made extensive modifications in the nonlinear block to implement our methods and strategies. We have also written the routines dealing with the triangular shell element.

The examples discussed below are solved using a VAX 11/780 or an APOLLO/DN300.

Only simple problems have been solved and presented in this report. They involve a limited number of d.o.f. (about 200). These examples are chosen in order to show the various possibilities of the present formulation to deal with pre and post-buckling and large rotations of arbitrary shells.

5.2 Nonlinear response of a 3D truss structure.

This example taken from [27] is chosen to show the possibility of the implemented numerical methods to deal with the automatic computation of very nonlinear problems. The 3D structure shown in Fig. 8 is made of 24 truss elements having 2 nodes and three d.o.f. per node (the 3 displacement components u, v, w). The structure is fixed at the base and subjected to a point load at the center 1 (in the u direction on Fig. 8). There are 21 active d.o.f.

A large number of runs have been performed with various parameters such as:

- TLF or ULF options
- arc-length with or without adjusting $\overline{\Delta S}_p$
- full N-R or modified N-R
- load value at the first step
- influence of the TEST of convergence in the numerical process

Some load-displacement curves are given on Figs. 9 and 10, where u is the displacement under the load P and v is the displacement in direction y at node 2. Figure 9 is obtained with the full N-R and the automatic arc-length method with no modification of arc-length (Eq. 88 is used with $\varepsilon = 10^{-3}$). The first nonlinear solution is obtained with a prescribed value of $\overline{P} = 10^4$ P/EA equal to 2. Then the arc-length $\overline{\Delta S}_p$ is computed using Eq. 93, i.e. $\overline{\Delta S}_p = < U^1 > \{ U^1 \}$. All symbols in Figure 9 coincide with equilibrium solutions obtained automatically. There are 8 limit points for the range of load and displacements considered and these curves correspond to the primary solution (with full symmetry). Of

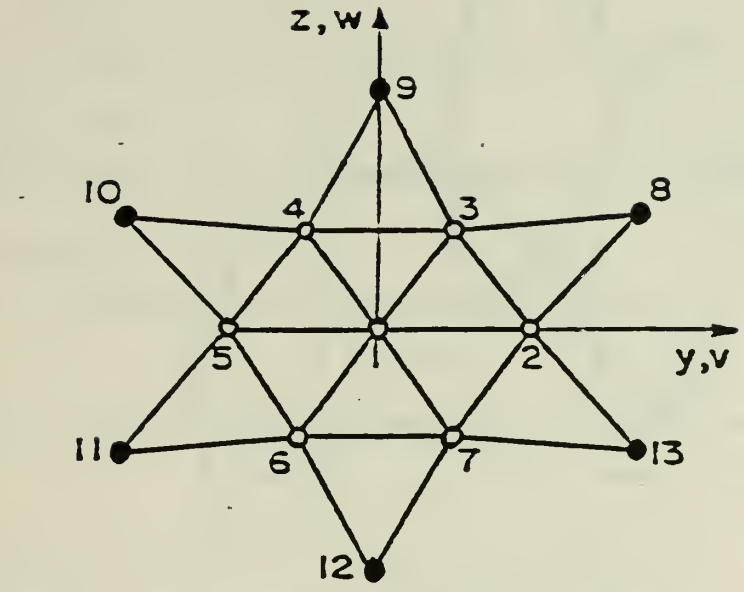

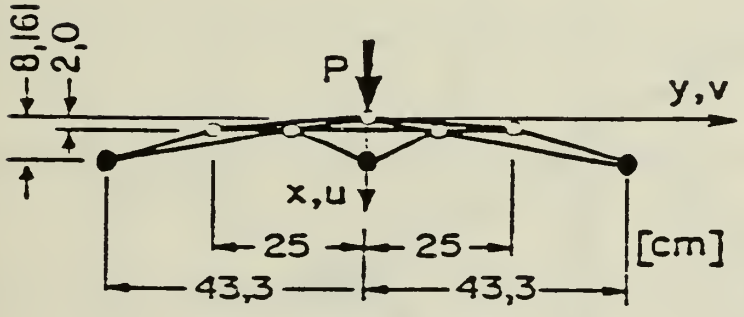

Figure 8 Three dimensional truss structure

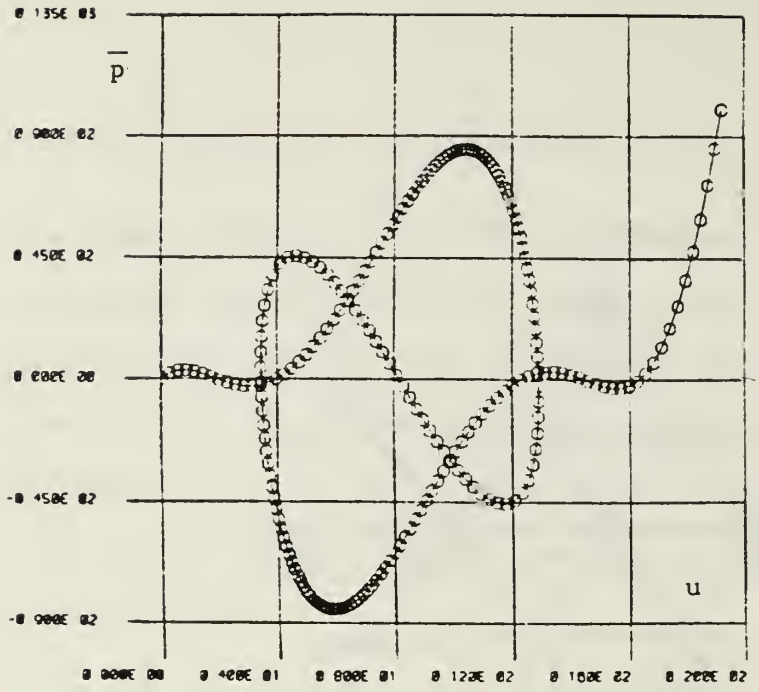

$\lambda^1 = 2$

Full N-R

$\Delta\bar{S}p$ constant

214 steps

461 iterations

a) P versus u

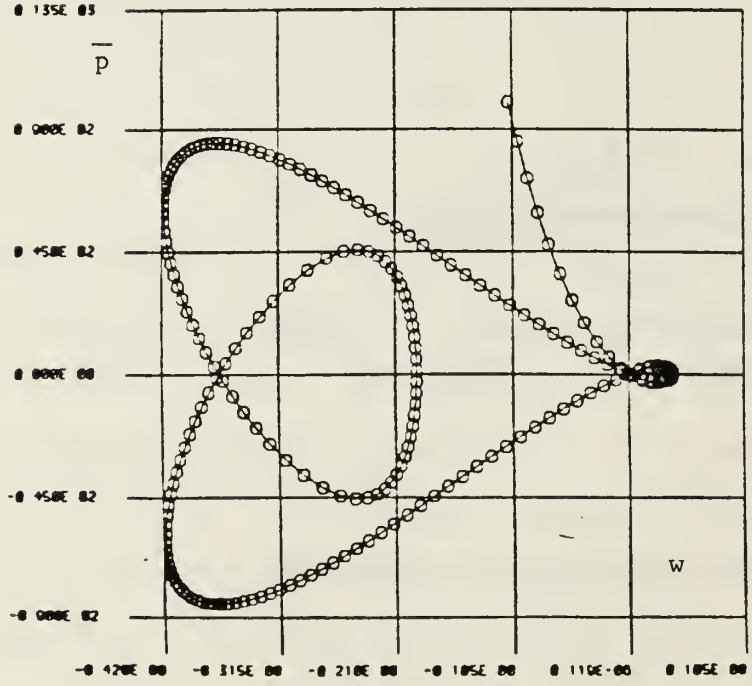

b) P versus w

Figure 9 Load deflection curves for 3D structure (constant arc-length)

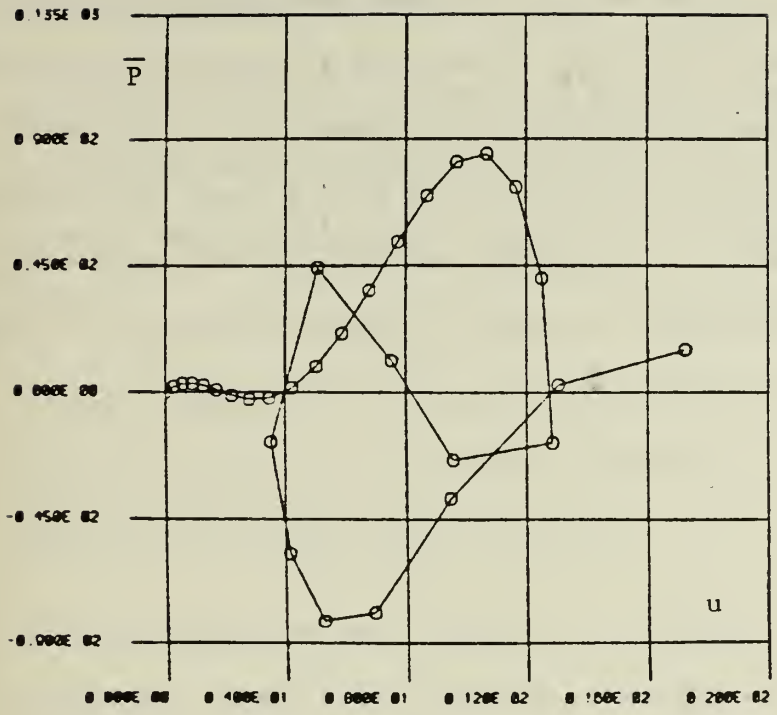

$\lambda^1 = 2$

Full N-R

$\Delta\overline{S}p$ variable

($\alpha = 0.5$, Id = 4

29 steps

99 iterations

a) $\overline{P}$ versus u

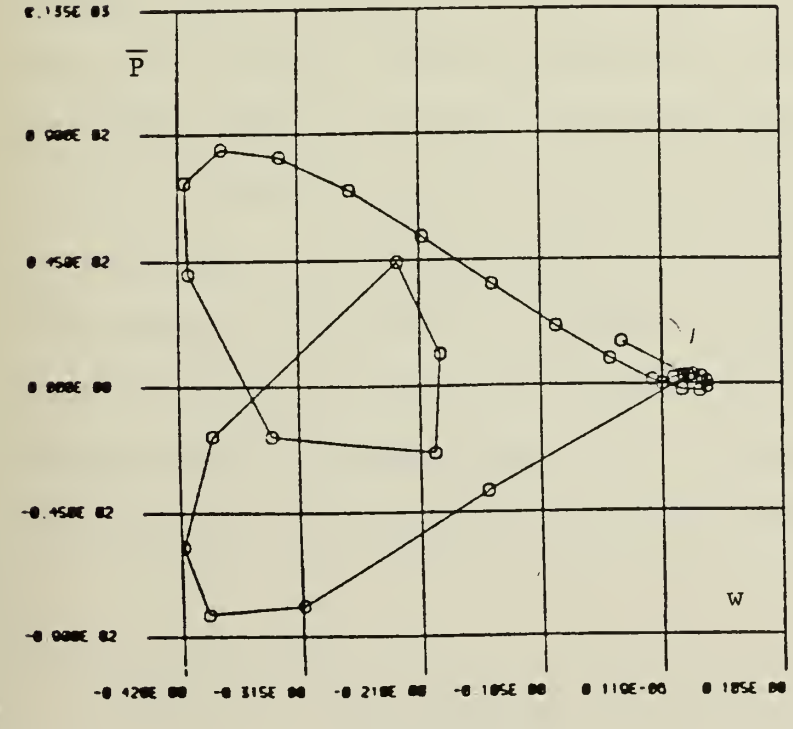

b) P versus w

Figure 10 Load Deflection Curves for 3D Truss Structure

(variable arc-length)

course there are other solutions which are associated with bifurcations. Figure 10 presents the solution in the case of automatic modification of the arc-length using Eq. 96 where $\alpha = 0.5$ and Id = 4. All points on Figure 10 correspond to solutions. This figure shows the robustness of the automatic computation algorithm when full N-R and arc-length methods are combined. Our results coincide with those presented in a recent paper [27].

5.3 Snap through the snap back of the cylindrical shell (CTEX4)

The problem presented in Figure 11 has been widely used in the literature to compare the performance of various nonlinear formulations, finite element models and nonlinear solution strategies. [18], [20], [28], [16].

A simple mesh of DKT18 elements was considered (48 elements, 210 dof before elimination of the imposed variables). The straight edges are hinged and the curved edges are free.

In this problem we have studied the influence of the formulation (TLF verse ULF), the influence of the arc-length strategy on the solution. The solutions have been obtained using the full N-R or the modified N-R method.

The influence of the formulation can be seen on Figures 12 and 13 where curves relate the load versus the normal under the load or at the free edge. (The results have been obtained with full N-R, with constant arc-length steps). The first solution was obtained for a prescribed load P = 1kN. Figures 12b and 13b are in good agreement with the "reference solution" as given by several authors. The TLF gives a higher value for the buckling load and doesn't reproduce the snap-back behavior for the central displacement for the small mesh considered. However it is expected that the correct answer will be obtained with the refinement of the mesh since this problem doesn't involve very large rotations.

The curves on Figure 14 are obtained using the modified N-R method, the ULF and a variable arc-length increment (with $\alpha = 0.5$ and Id = 4). The results are the correct ones and are obtained very efficiently in terms of computer time.

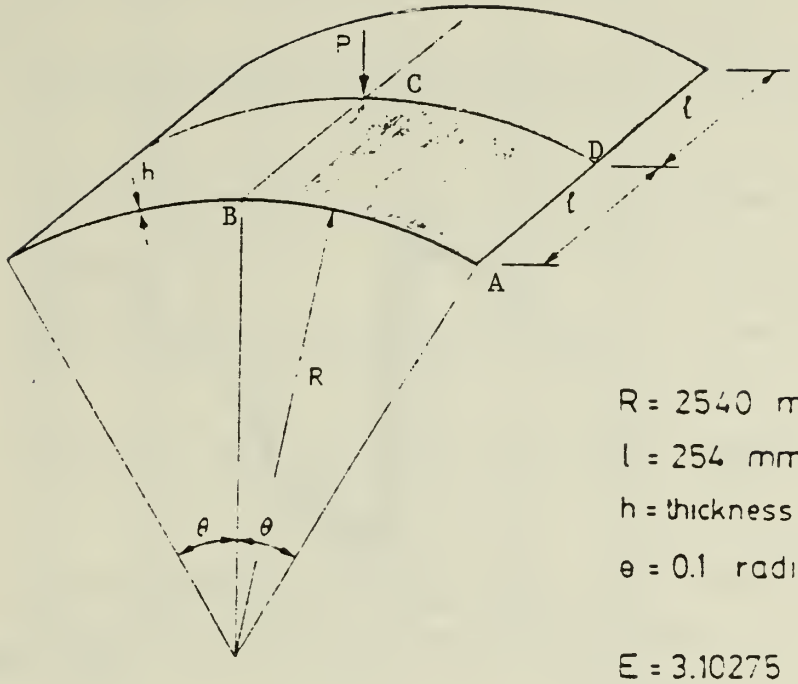

R = 2540 mm

ℓ = 254 mm

h = thickness = 6.35 mm

θ = 0.1 radians

E = 3.10275 kN/mm²

ν = 0.3

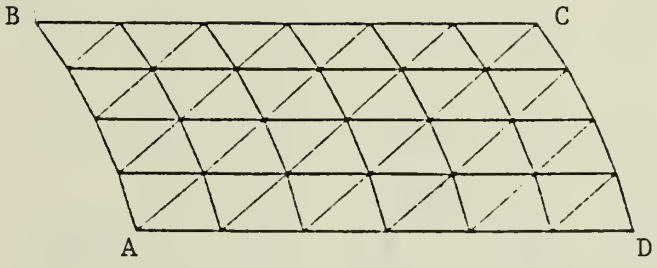

4 by 6 DKT18 mesh

Figure 11. Cylindrical shell with free curved edges and hinged straight edges (CTEX4)

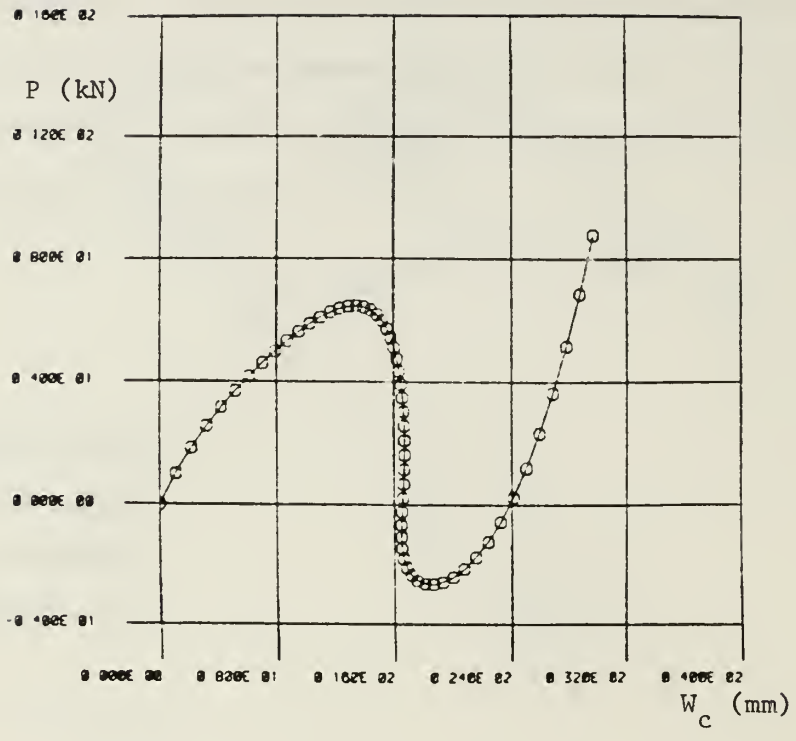

a) TLF

(Full N-R and constant arc-length)

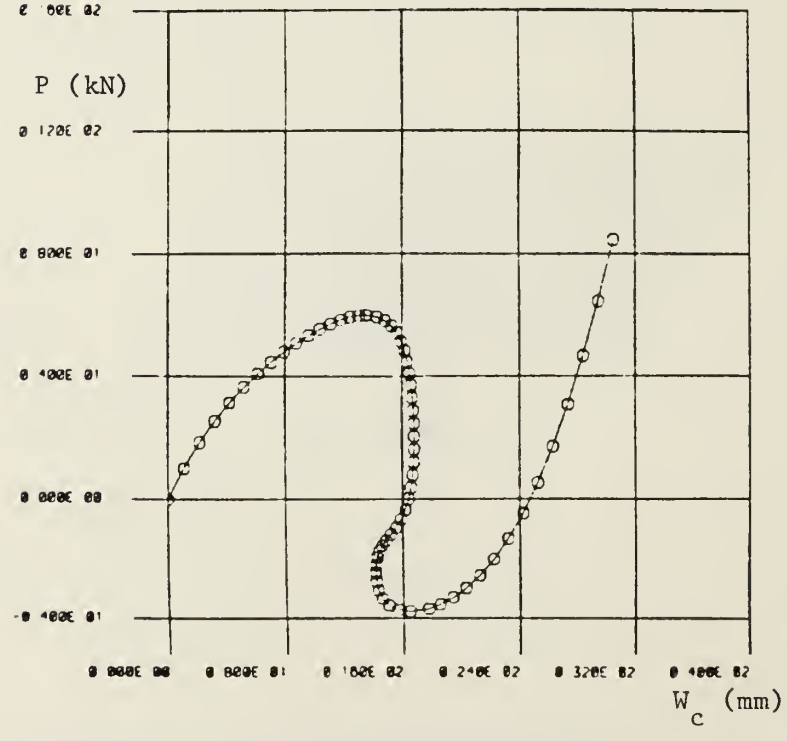

b) ULF

Figure 12 P versus W_c for CTEX4
TLF and ULF results

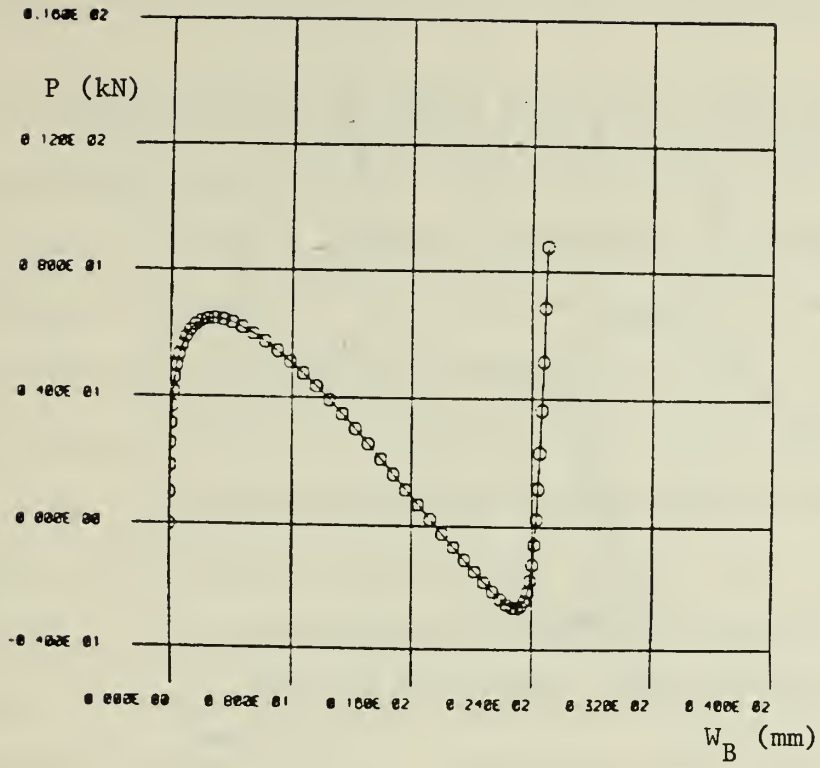

a) TLF

(Full N-R and constant arc-lengh)

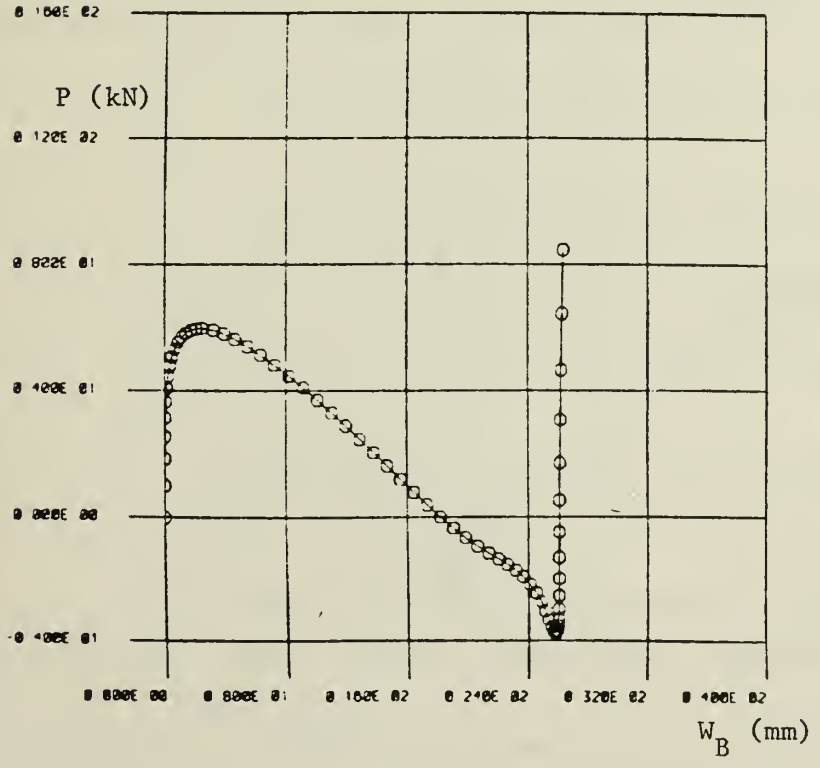

b) ULF

Figure 13. P versus W_B for CTEX4. TLF and ULF results

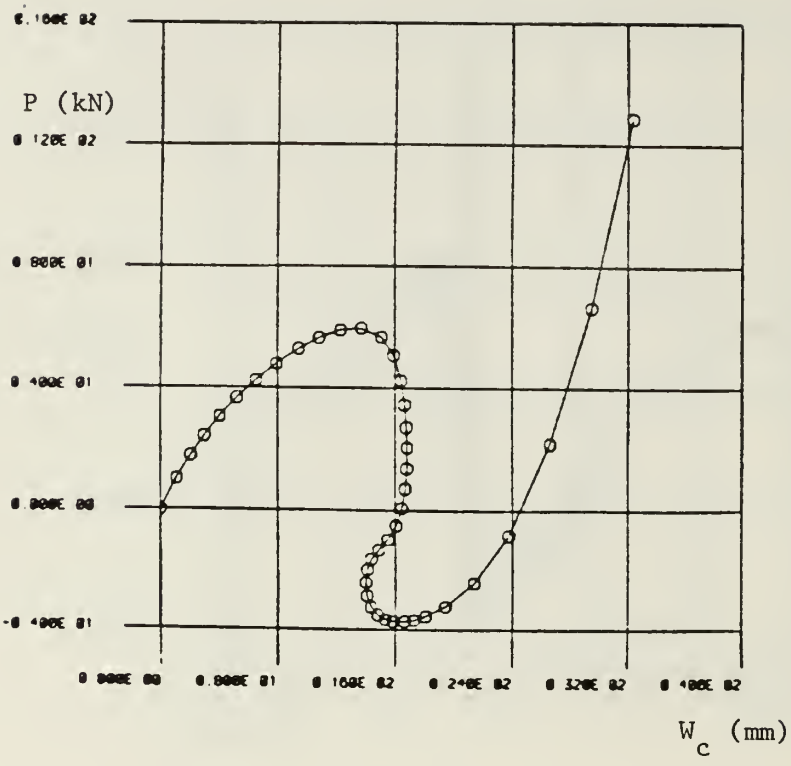

(variable arc-length α = 0.5, Id = 4

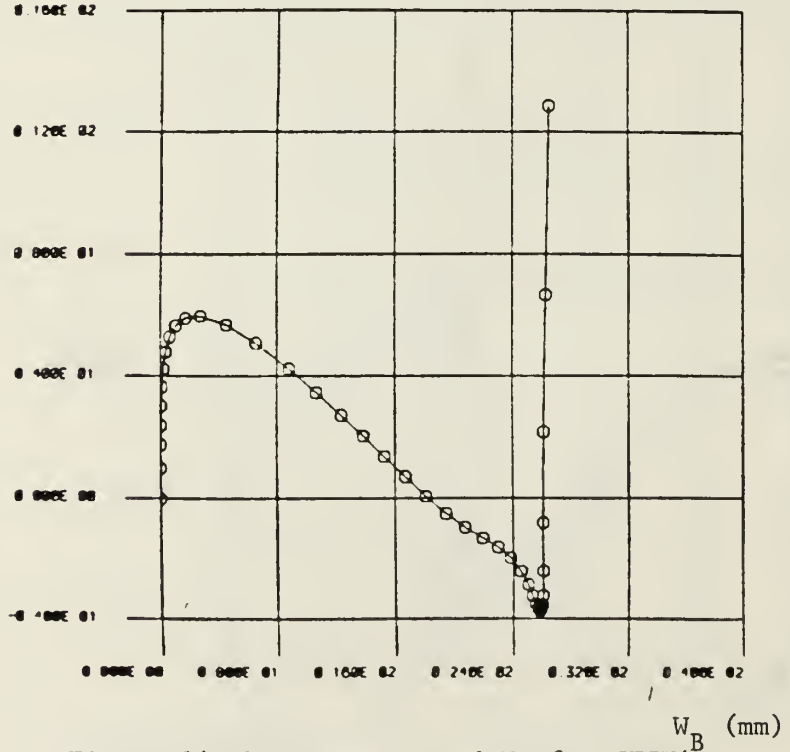

Figure 14 P versus W_c and W_b for CTEX4
ULF and modified N.-R.

5.4 Spherical cap

The problem presented on Figure 15 has also been considered by several researchers since 1969 [29], [20], [30], [31], [32]. The four edges are hinged and a load is applied at the center. A uniform mesh of 5 by 5 elements (50 elements, 216 d.o.f. before the elimination of the prescribed d.o.f.) has been considered.

The central deflection versus the load is given on Figure 16 for both TLF and ULF and using the imposed displacement and the full N-R methods (Eq. 91). The value $\Delta\overline{U}q$ is constant and equal to 0.2 h. The ULF gives good results, in agreement with the results given by other authors. The TLF leads to a slightly higher buckling load and doesn't represent the unstable branch properly. A finer mesh would result in better results using the TLF here since the displacements are only two times the thickness. The same type of results have been obtained using the arc-length algorithm with or without variable $\overline{\Delta S}_p$.

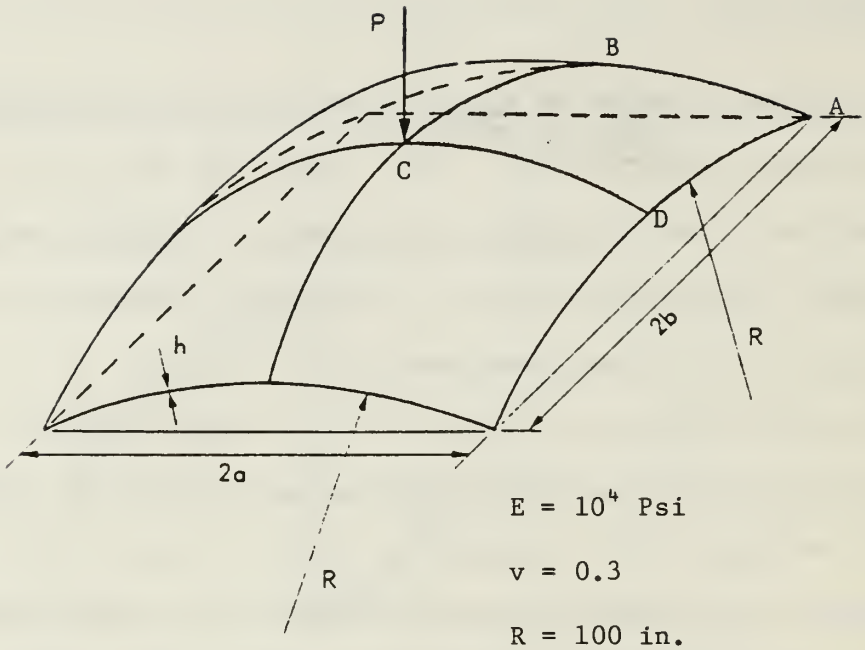

$E = 10^4$ Psi

$v = 0.3$

$R = 100$ in.

$a = b = 30.9017$ in.

$h = 3.9154$ in.

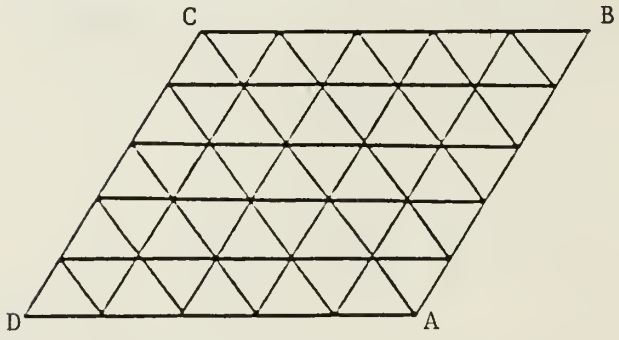

5 by 5 DKT18 mesh

Figure 15. Shperical cap

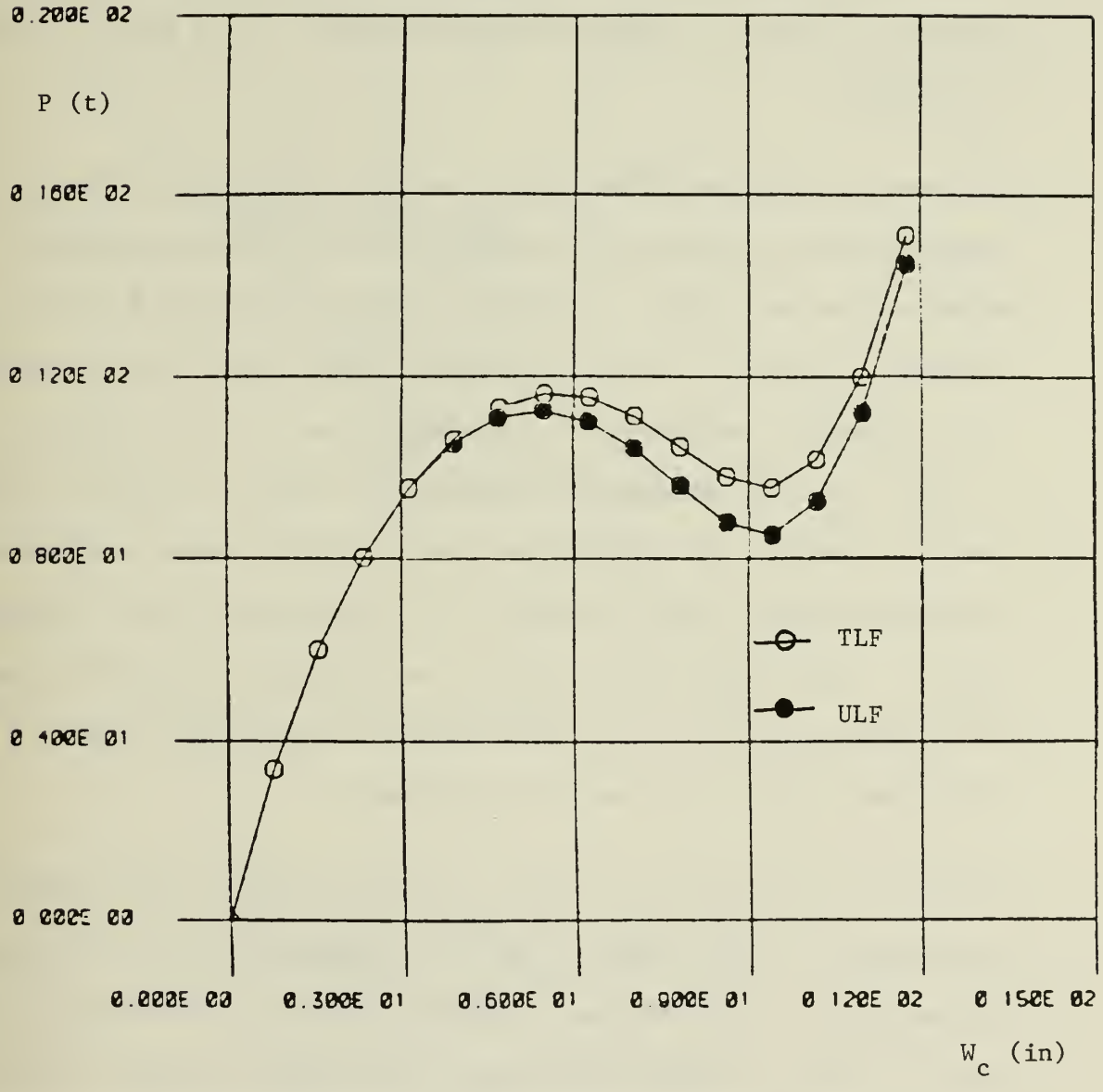

Figure 16. Spherical cap. Load versus central deflection for TLF and ULF

5.5 Cylindrical shell with clamped curved edges (CTEX1)

The membrane stiffening behavior of a cylindrical panel subjected to a central load with straight free edges and clamped curved edges, as described in Figure 17, has been studied with a 4 by 6 mesh for a quarter of the shell.

The central displacement versus the load is presented in Figure 18. The numerical results presented are obtained using load incrementation (constant increments $\overline{\Delta\lambda} = 1$ lb) and full N-R, for both TLF and ULF. With the TLF, the results are quite far from those of [33] using sophisticated cubic Lagrangian isoparametric elements (a mesh of 4 x 6 elements leading to 1200 d.o.f. was considered in [33]). The results using TLF elements cannot be improved by reducing the load increments since convergence has occurred and there is no influence of the load steps on the converging results. These results can, however, be improved by using finer meshes. The results with TLF are not good because we have fairly large displacements (up to 10 times the thickness).

For the same number of load steps, the ULF formulation gives better results than the TLF. This is due to the effect of large displacements and moderately large rotations. Improved results can be obtained with the ULF if the load steps are reduced. The correct results would be obtained if both the number of elements and the number of steps are increased.

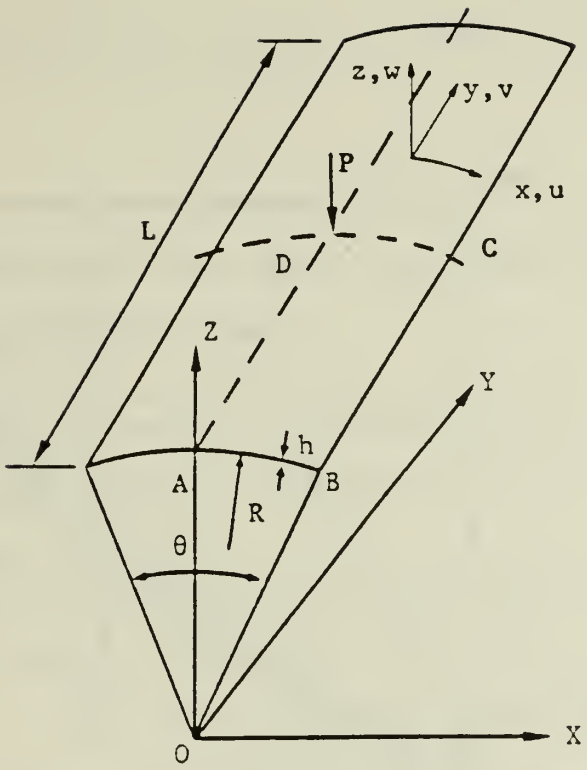

R = 2.5 in.

L = 6 in.

h = 0.01 in.

θ = 45

E = 10^7 psi

ν = 0.3

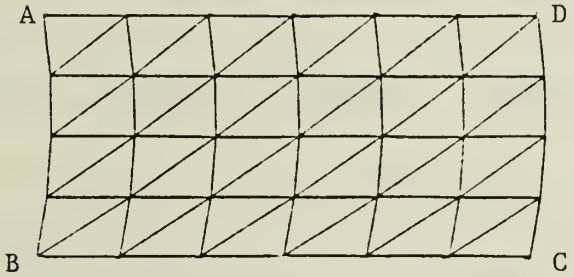

4 by 6 DKT 18 mesh

Figure 17. Cylindrical shell with straight edges free

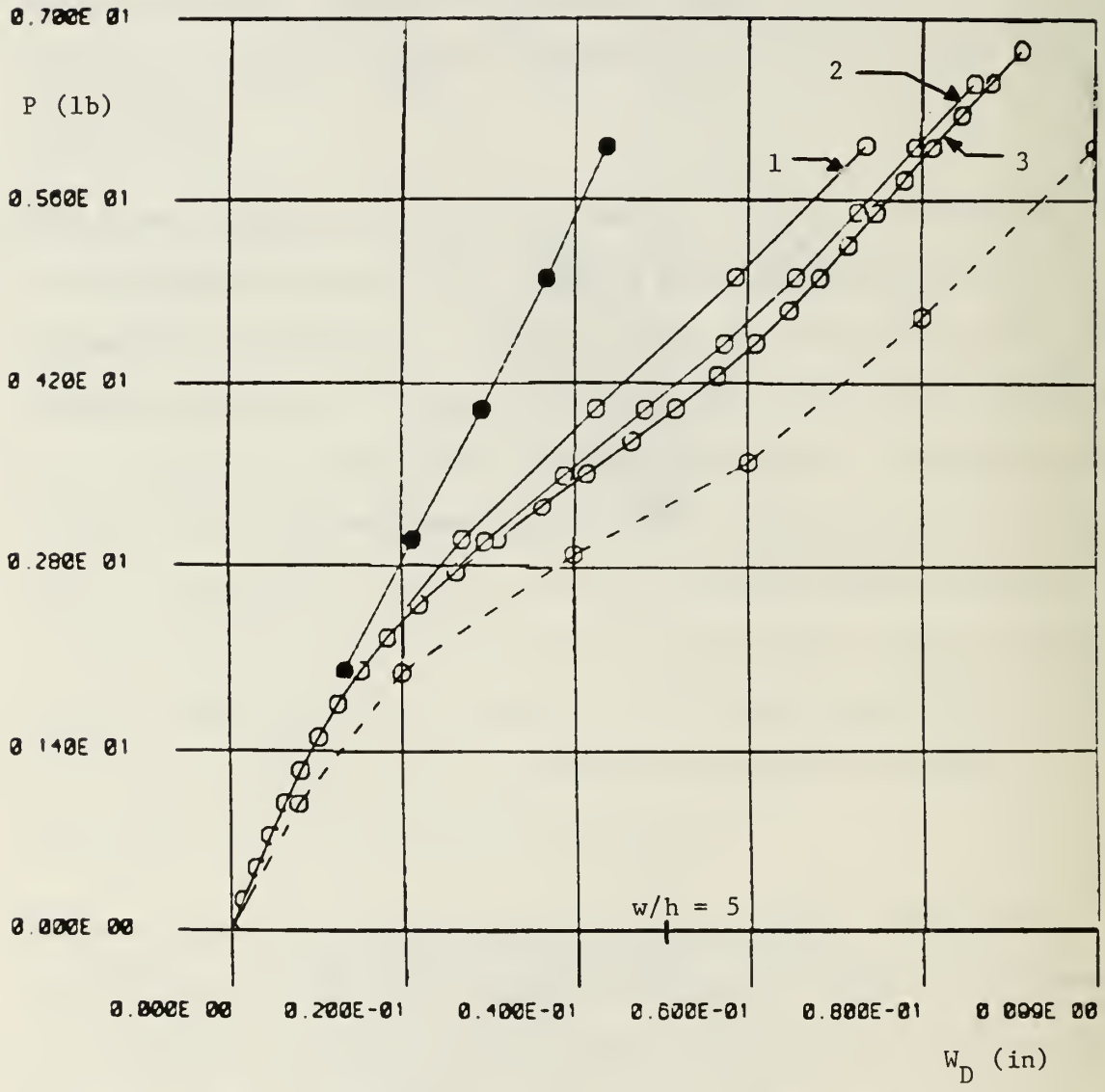

Figure 18. Cylindrical shell CTEX1
Influence of the formulations

5.6 Far post-buckling of a cylindrical shell with hinged curved edges (CTEX2)

The shell structure presented in Figure 17 is again considered but with hinged conditions on the curved edges (these edges are not restrained in the axial direction).

In this case the behavior is different from the clamped case since the displacements are much larger for the same load and snap through occurs for a load of 2.3 lbs.

The same type of analysis as in the clamped case has been performed for $0 < W/h < 14$ using now the prescribed displacement algorithm for various $\Delta\bar{U}q = \Delta w_D$ and again the full N-R method. The results are presented in Figure 19 for the TLF and the ULF (7 and 14 steps). The inability of the TLF to find a limit load is clearly shown in the figure. Again better results would need much more elements. The ULF leads to good results with a limit load 20% higher than the reference value taken from [33] with 28 steps. A more accurate value would need more d.o.f.'s.

The response of the shell for very large displacements and rotations has also been studied for the same mesh. Figure 20 shows P versus the central displacement up to 150 times the thickness (and 1/4 of the length) using 70 steps, the ULF, full N-R and the displacement control algorithm. The slight oscillations observed on Figure 20 are due to the fact that in the regions considered the overall tangent matrices are very ill-conditioned. The influence of the type of representation of $[\underset{\sim}{k}_{\theta_z}]$ in these regions is important. If the displacement increments are reduced, these oscillations disappear and the behavior is slightly

different as shown in Figure 21 where 140 steps are considered. One can observe on this figure the low post-buckling minimum and a second snap-through for $W/j \simeq 90$ which corresponds to a local deformation of the cross-section near the boundary. The results presented in Figure 21 are in good agreement with those reported in [33], the most important difference being in the evaluation of the first buckling load as shown on Figure 20.

The above results have also been obtained using the automatic variable arc-length algorithm combined with the full N-R method. This example has clearly shown the capability of the formulation to deal with large rotations.

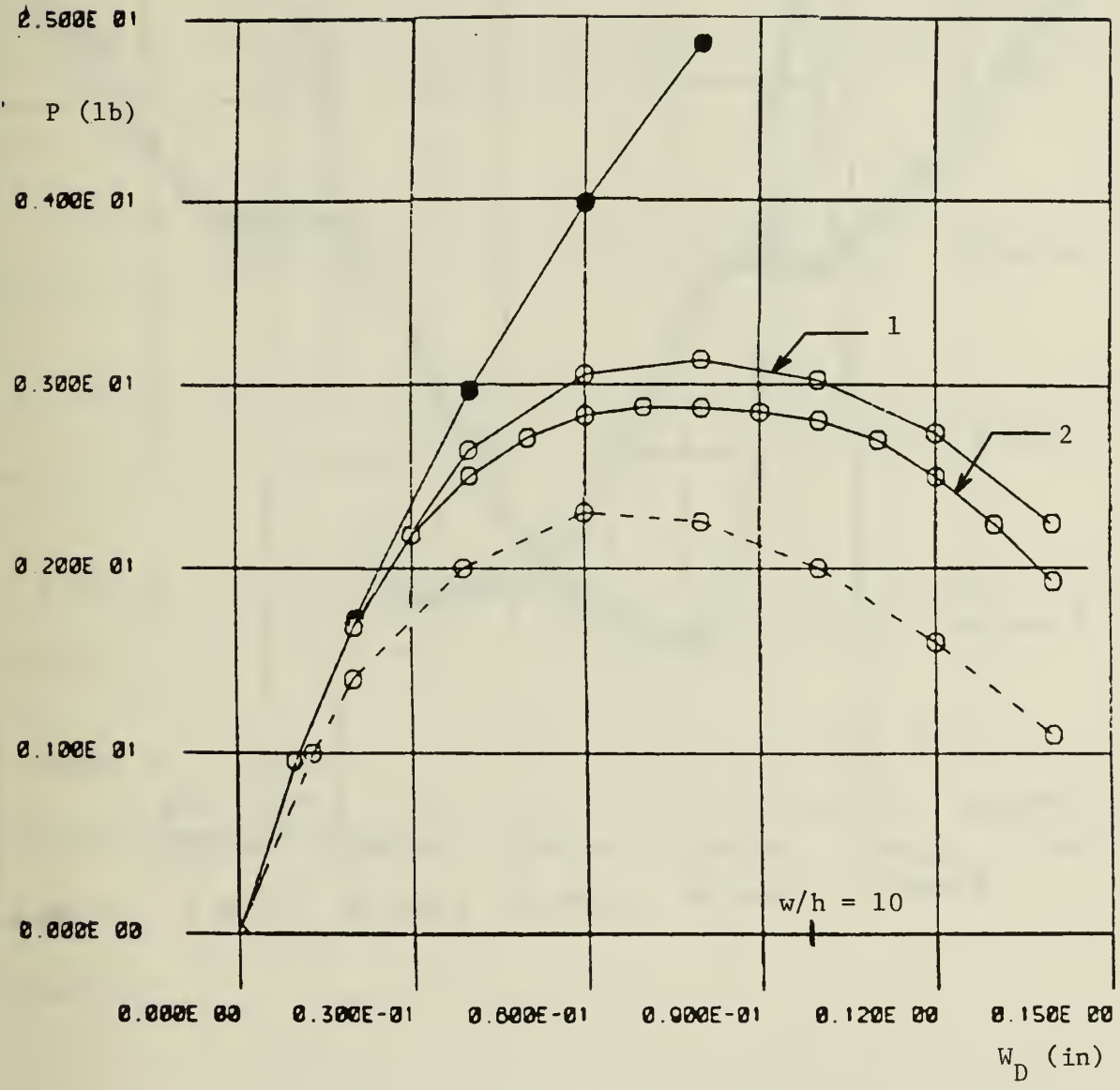

DKT18, TLF

DKT18, ULF (1 : 7 steps, 2 : 14 steps)

Ref. 33, ≈1000 dof

Figure 19 Cylindrical Shell CTEX2 (Influence of the formulations)

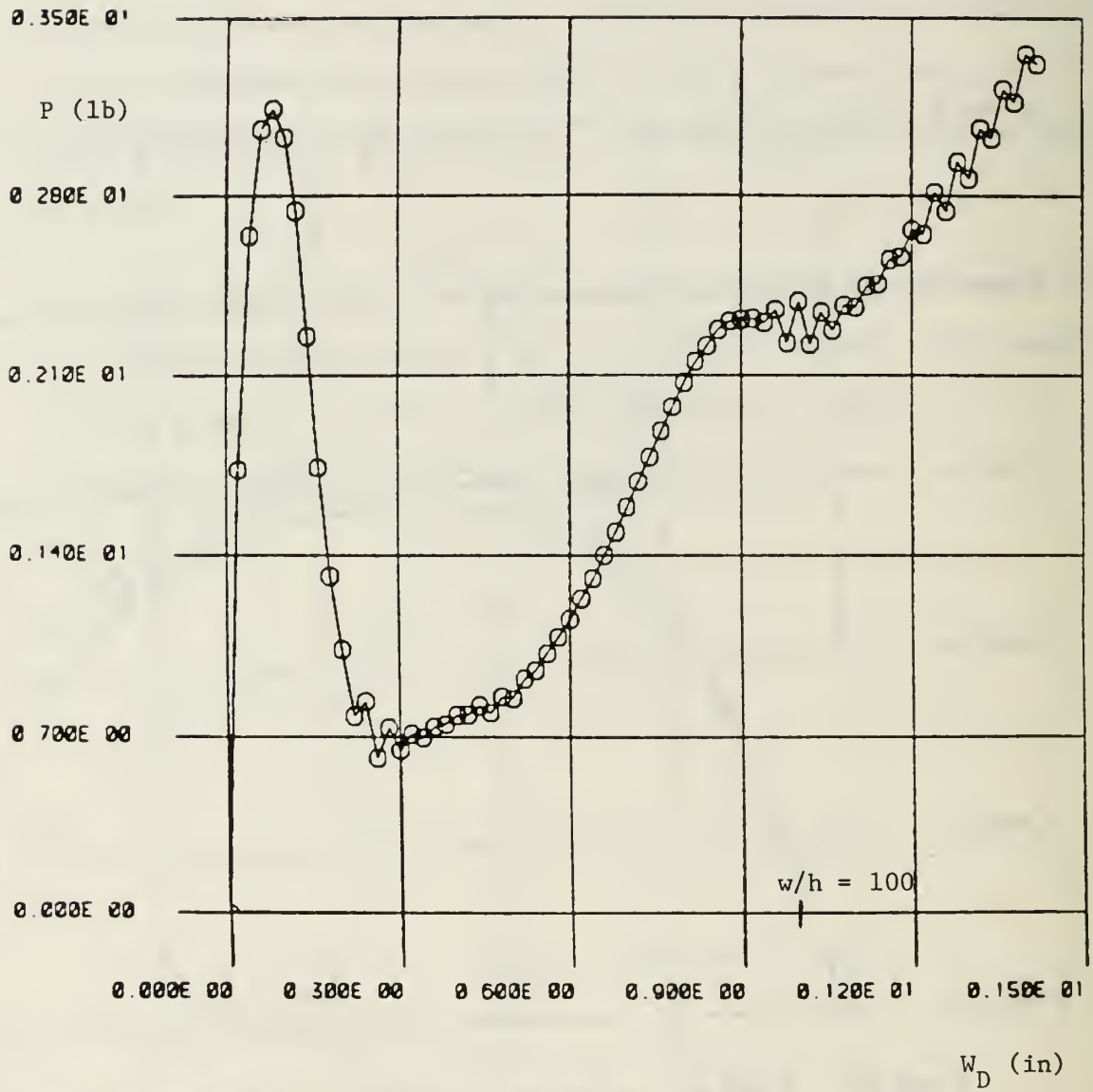

Figure 20. Cylindrical shell CTEX2
Far post-buckling (ULF, 70 steps)

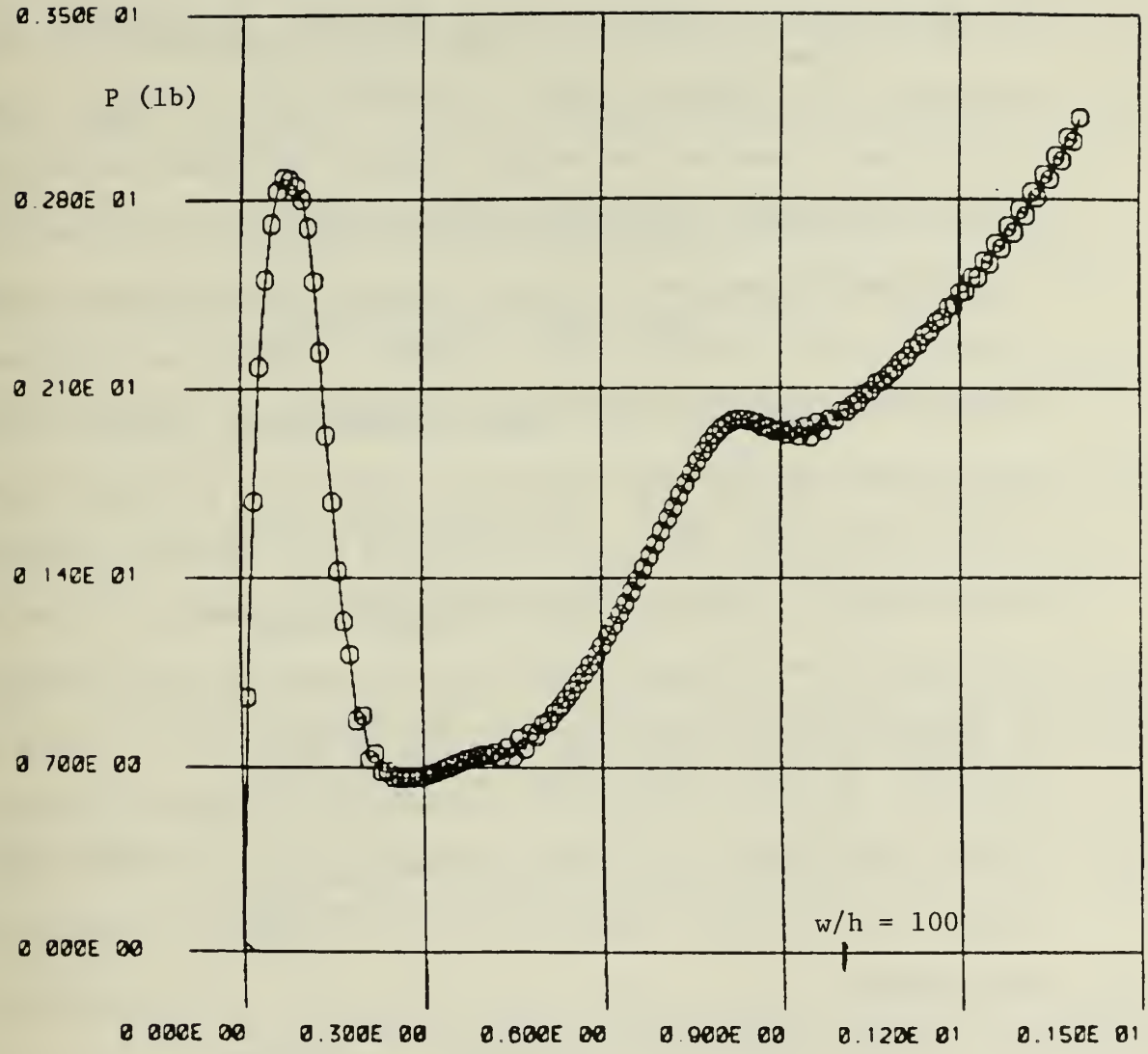

Figure 21. Cylindrical shell CTEX2
Far post-buckling (ULF, 140 steps)

6. CONCLUSIONS

The numerical results presented in this report have shown the ability of the DKT18 elements combined with the ULF to give accurate and efficient answers to very different types of nonlinear shell problems including snap-through, snap-back situations and large rotations post-buckling. The three automatic strategies have been tested and it is found that the full N-R method combined with the arc-length method are very reliable and powerful to deal with all kinds of nonlinear situations. The overall package can solve moderately large problems on mini and micro-computers. This package has several capabilities since it has retained different aspects such as TLF, ULF, full or modified N-R, automatic constant or variable load or displacement or arc-length increments,... The modules dealing with the nonlinear procedures and the DKT18 shell elements can be adapted to other finite element codes having a similar structure than MEF [19]. Also, the procedures are independent of the DKT18 shell element; therefore, the library of elements can be enriched in the future. Elasto-plastic behavior can also be included if small strains are assumed.

ACKNOWLEDGEMENTS

This research has been supported by NSRDC, Washington, D.C., and has benefited from continous exchanges between the Université de Technologie de Compiègne, France, Université Laval, Québec, Canada and the Naval Postgraduate School, Monterey, USA.

7. REFERENCES

[1] Bushnell, D., "Buckling of Shells-Pitfall for Designers", AIAA, Vol. 19, no. 3, Sept. 1981, pp. 1183-1226.

[2] Sobel, L., Thomas, K., Eds., "Collapse Analysis of Structures", PVP, Vol. 84, ASME, 1984.

[3] Bathe, K. J., Finite Element Procedures in Engineering Analysis, Prentice-Hall, Englewood Cliffs, New Jersey, 1982.

[4] Washizu, K., Variational Methods in Elasticity & Plasticity, (3rd Edition), Pergamon Press, 1982.

[5] Malvern, L., "Introduction to the Mechanics of a Continuous Medium", Prentice-Hall, 1969.

[6] Batoz, J. L., Bathe, K. J., Ho, L. W., "A Study of Three Node Triangular Plate Bending Elements", IJNME, Vol. 15, pp. 1771-1812, 1980.

[7] Batoz, J. L., "An Explicit Formulation for an Efficient Triangular Plate Bending Element", IJNME, Vol. 18, pp. 1077-1089, 1982.

[8] Batoz, J. L., Dhatt, G. S., "An Evaluation of Two Simple and Effective Triangular and Quadrilateral Plate Bending Elements", New and Future Developments in Commercial Finite Element Method, J. Robinson Ed., Los Angles, Oct. 1981, pp. 352-368.

[9] Bathe, K. J., Dvorkin, E. N., and Ho, L. W., "Our Discrete-Kirchhoff and Isoparametric Shell Elements for Nonlinear Analysis - An Assessment" J. Computers and Structures, Vol. 16, pp. 89-98, 1983.

[10] Bathe, K. J., Ho, L. W., "Some Results in the Analysis of Thin Shell Structures", Nonlinear Finite Element Analysis in Structural Mechanics, (edited by W. Wunderlich et al), Springer-Verlag, Berlin, 1981.

[11] Jaamei, S., "Analyse nonlineaire et grandes rotations de coques minces", Ph.D. Thesis, UTC, France (to appear).

[12] Batoz, J. L., Dhatt, G. S., "Incremental Displacement Algorithms for Nonlinear Problems", Int. Journal for Numerical Methods in Eng., Vol. 14, pp. 1262-1266, 1979.

[13] Powell, G., Simons, J., "Improved Iteration Strategy for Nonlinear Structures", IJNME, Vol. 17, 1981, pp. 1455-1467.

[14] Riks, E., "The Application of Newton's Method to the Problem of Elastic Stability", J. Appl. Mechanics, Vol. 39, 1972, pp. 1060-1066.

[15] Wempner, G. A., "Discrete Approximations Related to Nonlinear Theories of Solids", Int. J. Solids Structures, Vol. 7, 1971, pp. 1581-1599.

[16] Ramm, E., "Strategies for Tracing the Nonlinear Response Near Limit Points", Nonlinear FE Analysis in Structural Mechanics, Springer-Verlag, New York, 1981, pp. 68-89.

[17] Crisfield, M. A., "An Arc-Length Method Including Line Search and Accelerations", Int. J. for Num. Methods in Eng., Vol. 19, 1983, pp. 1269-1289.

[18] Crisfield, M., "Numerical Analysis of Structures", Chapt. 7 of Developments in Thin-Walled Structures-1, Ed. Rhodes and Walker, Applied Sciences Publishers Ltd., pp. 235-284, 1981.

[19] Dhatt, G. S., Touzot, G., "The Finite Element Method Displayed", translated in English by G. Cantin, John Wiley, 1984.

[20] Horrigmoe, G., "Finite Element Instability Analysis of Free-Form Shells", Report no. 77-2, May 1977, The Norwegian Institute of Technology.

[21] Wunderlich, W., Stein, E., Bathe, K. J., eds., "Nonlinear Finite Element Analysis in Structural Mechanics", Springer-Verlog, 1981.

[22] Batoz, J. L., Ben Tahar, "Un element de coque mince triangulaire", Rapport UTC/GM/MNM, Mars 1982.

[23] Zienkiewicz, O. C., The Finite Element Method (3rd Edition), McGraw-Hill, 1977.

[24] Bergan, P. G., Holand, I., Soreide, T. H., "Use of Current Stiffness Parameter in Solution of Nonlinear Problems", Energy Methods in Finite Element Analysis, ed. by R. Glowinski, E. Y. Rodin and O. C. Zienkiewicz, John Wiley & Sons Ltd, 1979, pp. 265-282.

[25] Haisler, W. E., Stricklin, J. A., "Displacement Incrementation in Nonlinear Structure Analysis by the Self-Correcting Method", IJNME, Vol. 11, 1977, pp. 3-10.

[26] Bathe, K. J., Dvorkin, E. N., "On the Automatic Solution of Nonlinear as Finite Element Equations", Computers and Structures, Vol. 17, No. 5-6, 1983, pp. 871-879.

[27] Watson, L. T., Holzer, S. M., "Quadratic Convergence of Crisfield's Method", Computers and Structures, Vol. 17, No. 1, 1983, pp. 69-72.

[28] Sabir, A. B., Lock, "The application of finite elements to the large deflection geometrically nonlinear behavior of cylindrical shells", Variational Methods in Engineering, Brebbia and Tottenham eds, Southampton University, 1973, pp. 66-75.

[29] Dhatt, G. S. "Instability of Thin Shells by the Finite Element Method", Proc. IASS Conference, Vienne, 1970.

[30] Tahiani, C., Lachance, L., "Linear and Nonlinear Analysis of Thin Shallow

Shells by Mixed Finite Elements", Computers and Structures, Vol. 5, p. 167, 1977, 1975.

[31] Gallagher, R., "The Finite Element Representation for Thin Shell Instability Analysis", Buckling of Structures, Budiansky, Ed., Springer-Verlag, 1976, pp. 40-51.

[32] Carnoy, E., "Etude de la Stabilite elastique des conques par elements finis", These de doctorat, Université de Liège, 1980.

[33] Brendel, B., Ramm, E., "Linear and Nonlinear Stability Analysis of Cylindrical Shells", Computers and Structures, Vo. 12, pp. 549-558, 1980.

INITIAL DISTRIBUTION LIST

		No. Copies
1.	Defense Technical Information Center Cameron Station Alexandria, Virginia 22314	2
2.	Library, Code 0142 Naval Postgraduate School Monterey, California 93943-5100	2
3.	Chairman, Code 69Mx Department of Mechanical Engineering Naval Postgraduate School Monterey, California 93943-5100	1
4.	Professor Gilles Cantin, Code 69Ci Department of Mechanical Engineering Naval Postgraduate School Monterey, California 93943-5100	4
5.	Professor Ramesh Kolar, Code 67 Department of Aeronautics Naval Postgraduate School Monterey, California 93943-5100	1
6.	Professor K. J. Bathe Department of Mechanical Engineering Massachusetts Institute of Technology 77 Massachusetts Avenue Cambridge, Massachusetts 02139	1
7.	Professor Edward L. Wilson Structural Engineering Division Department of Civil Engineering University of California, Berkeley Berkeley, California 94720	1
8.	Dr. Gilbert Touzot U.T.C. Université de Technologie 60206 Compiègne Cedex, FRANCE	1
9.	Professor Guri Dhatt Centre Technique de l'Informatique Université Laval Québec, Prov. de Québec CANADA G1K/P4	

10. Dr. Jean Louis Batoz
U.T.C.
Université de Technologie
60206 Compiègne Cedex, FRANCE — 1

11. Professor Thomas Hughes
Division of Applied Mechanics
Room 283 Durand
Stanford, California 94305 — 1

12. Professor Ted Belytschko
Civil and Nuclear Engineering
Northwestern University
Technological Institute
Evanston, Illinois 60201 — 1

13. Dr. Rem Jones, Code 172
David W. Taylor Naval Ship
Research and Development Center
Bethesda, Maryland 20084 — 1

14. Dr. Alan Kushner, Code 4325
Office of Naval Research
800 North Quincy Street
Arlington, Virginia 22217 — 1

15 Dr. Charles Rankin
Lockheed Corporation
3251 Hanover Street
Palo Alto, California 94304 — 1

16. Dr. K. C. Park
Lockheed Corporation
3251 Hanover Street
Palo Alto, California 94304 — 1

17. Mr. Joseph Carrado, Code 1702
David W. Taylor Naval Ship
Research and Development Center
Bethesda, Maryland 20034 — 1

18. Mr. J. Niemiec, Code 1965
David W. Taylor Naval Ship
Research and Development Center
Bethesda, Maryland 20034 — 1

19. Mr. R. A. Langworthy
Applied Technology Laboratories
U.S. Army Research and Technology Laboratory
Fort Eustis, Virginia 23604 — 1

20. Dr. E. M. Lenoe 1
U.S. Army Materials Technology Laboratory
Arsenal Street
Watertown, Massachusetts 02122

21. Dr. Roshdy Barsoun 1
U.S. Army Materials Technology Laboratory
Arsenal Street
Watertown, Massachusetts 02122

22. Dr. D. Hibbitt 1
Hibbitt, Karlsson and Sorensen, Inc.
35 South Angell Street
Providence, Rhode Island 02906

23. Research Administration Office 1
Code 012
Naval Postgraduate School
Monterey, CA 93943